工學博士學位論文

Fabrication of Sinter-free Conductive Paste based on Cu Nanomaterials

구리 나노물질 기반 비소결식 전도성 페이스트의 제조와 응용

2018年 2月

서울大學校 大學院

化學生物工學部

李 政 燮

Fabrication of Sinter-free Conductive Paste based on Cu Nanomaterials

구리 나노 물질 기반 비소결식 전도성 페이스트의 제조와 응용

指導敎授 張 正 植

이 論文을 工學博士 學位論文으로 提出함
2017 년 11 월
서울大學校 大學院
化學生物工學部
李 政 燮

李政燮의 工學博士 學位論文을 認准함
2017 年 11 月

委 員 長 _____ (인)

副委員長 _____ (인)

委 員 _____ (인)

委 員 _____ (인)

委 員 _____ (인)

Fabrication of Sinter-free Conductive Paste based on Cu Nanomaterials

by

Jungsup Lee

Submitted to the Graduate School of Seoul National University in Partial Fulfillment of the Requirements for the Degree of Doctor of Philosophy

February, 2018

Thesis Adviser: Jyongsik Jang

Abstract

Printed electronics became one of the most promising application for fabrication of electronic devices. Especially, manufacturing flexible electronics proved attractive in that it could be applied to numerous practical application. However, conventional methods require expensive equipment and high cost manufacturing process. Therefore, the printed electronics, which utilizes conductive ink is getting large attention as it is cost-efficient and fast. Conductive ink is usually composed of conductive material, liquid base, and various additives. Especially, metal nanomaterials have drawn considerable attention as conductive materials due the modern wet chemical technology which enabled the large-scale production. Typically, silver nanoparticles-based inks are widely utilized these days due to the high conductivity. However, high cost of silver makes the real life application of conductive ink difficult.

This dissertation provides conductive paste based on cheap Cu nanomaterials. Cu nanoparticles and nanowires are used as solid loadings for the conductive paste. Also, the printed pattern does not require thermal or photo sintering process, which could reduce the

manufacturing cost. Moreover, sinter-free conductive paste enables to use substrate which is weak to heat or light.

Cu nanoparticles and nanowires are synthesized by wet-chemical method and hydrothermal method respectively. Cu nanowires are utilized to substitute conventional carbon paste and used as dual functional materials; conductive paste and glucose sensor. Cu nanoparticles were synthesized to enhance the conductivity of the sinter-free conductive paste. Moreover, Cu nanoparticles were mixed with Cu nanowires to increase the sinter-free conductive paste.

The sinter-free conductive paste presented in this dissertation could be applied to various fields such as printed circuit boards, RFID tags, thin film transistors, light emitting devices, solar cells, transparent electrodes, and flexible displays. In addition, this dissertation might not only provide synthetic route for Cu nanomaterials based conductive paste but open a new path on fabricating sinter-free conductive paste

Keywords: Cu nanomaterials, conductive paste, sinter − free, flexible, glucose sensor, dipole tag antenna

Student Number: 2013-22534

List of Abbreviations

1D: one-dimension

Ag/AgCl electrode: silver chloride electrode

Cu: copper

fcc: face-centered-cubic

FE-SEM: field emission-scanning electron microscopy

FT-IR: fourier transform-infrared

GOx: glucose oxidase

HR-TEM: high resolution-transmission electron microscopy

hr: hour

min: minute

NaOH: sodium hydroxide

nm: nano-meter

NP: nanoparticle

NW: nanowire

R_0: initial resistance

TEM: transmission electron microscopy

XPS: x-ray photoemission spectroscopy

XRD: x-ray diffraction

ΔR: resistance change

μm: micro-meter

List of Figures

curves of carbon paste sensor strip and Cu NW strip in 0.1 M NaOH solution (scan rate: 50 mV s^{-1}).

Figure 12. CV curves of CuNW paste sensor strip in 0.1 M KCl and 5 mM $K_3[Fe(CN)_6]$ with various scan rates from 10 to 200 mV s^{-1}

Figure 13. (a) CV curves of Cu NW strip in 0.1 M NaOH solution with various glucose concentrations from 1 nM to 100 mM (scan rate: 50 mV s^{-1}). (b) CV curves of Cu NW strip in 0.1 M NaOH solution with 10 μM of glucose at various scan rates from 10 to 200 mV s^{-1}. (c) Amperometric responses of Cu NW strip on the successive injection of different concentration of glucose in 0.1 M NaOH solution (applied potential: 0.65 V). (d) Calibration plot of amperometric current response as a function of different concentration of glucose.

Figure 14. Amperometric selectivity response of Cu NW strip toward non-target (0.1 M NaCl, 10 μM ascorbic acid (AA), 10 μM Uric acid (UA), 10 μM dopamine (DA), 10 μM sucrose) and target (glucose) analytes (applied potential: 0.65 V).

List of Tables

Table of Contents

1. Introduction

1.1. Background

1.1.1. Fabrication of Copper-based Nanomaterials

1.1.1.1. Fabrication of Copper-based Nanoparticles

Metal nanoparticles have attracted considerable interest due to its unique features. The chemical and physical properties of the metal nanoparticles vary upon the size of the particle, making it a promising material in many application fields. Among various metal nanoparticles, copper has been extensively studied these days due to relatively low cost compared to gold and silver. Copper nanoparticles have shown its potential for diverse applications such as catalysis, optics, electronics, antimicrobial agents, or conductive ink.[1-8] However, stability and reactivity makes the application of copper nanoparticles in nano-device considerably difficult . Therefore, lot of efforts have been given to optimizing the stability of the copper nanoparticles as well as controlling its properties, such as morphology, size, and dispersity.[7, 9, 10]

There are generally two methods to prepare metal nanoparticles, “top-down” and “bottom-up” methods. The bottom-up methods became more

popular for fabrication of copper nanoparticles because it provides more efficient ways to control the shape and size of the particles. Bottom-up method to synthesize copper nanoparticles could include chemical, electrochemical, photochemical, sonochemical, and thermal method. Among the synthesizing method, chemical method have been widely used for ease of fabrication. Also, chemical method could be divided into several fabrication method; wet chemical method, reverse micelle method, and microwave assisted method. [11-13]

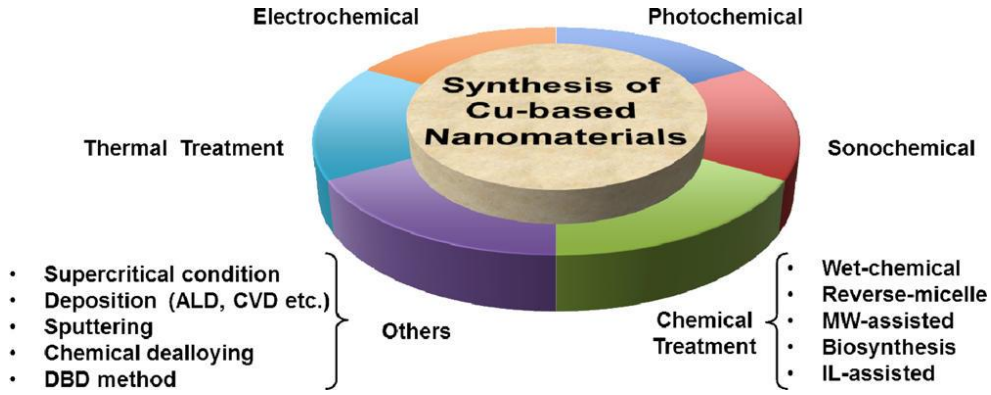

Figure 1. Major approaches to synthesize Cu-based nanomaterials**. [14]**

1.1.1.1.1. Wet chemical method

Wet chemical methods have long been used in the fabrication of Cu-based nanoparticles. It uses the reducing agents to reduce the copper salts to fabricate metallic copper. The copper salts include $CuSO_4$, $CuCl_2$, or $Cu(NO_3)_2$, and reducing agents include sodium borohydride, hydrazine, glucose, or ascorbic acid. Also, to control the size of the copper nanoparticles, diverse capping agents were utilized in the synthesizing process.

1.1.1.1.2. Reverse micelle method

Reverse micelle method were used as alternative approach to wet chemical method. It utilizes surfactant to create oil-in-water type micro-emulsion within solvent. Nanoparticles could be fabricated inside these reverse micelles with controlled size and shape. Using different size of micelles could result in different size of nanoparticles. Chen et al. used SDS as surfactant to create microemulsion system, synthesizing metallic Cu nanoclusters. [15]

1.1.1.1.3. Microwave assisted method

Microwave assisted method is rather new approach to fabricating copper nanoparticles. It uses microwave to utilize the microwave energy in synthesis process. The reaction process is stimulated by heat energy, which is converted from electromagnetic energy. Microwave assisted method is better compared to conventional method in that heat could be selectively given to the designated materials quickly, leading to high reaction speed and yield. Kawasaki et al. fabricated 2 nm Cu nanocrystals using microwave assisted method. They utilized non-aqueous solvent to avoid oxidation of the Cu surface. [16] Also, Yin et al. utilized rapid microwave assisted method to synthesize Cu nanoparticles using copper sulfate as precursor. [17]

1.1.1.2. Fabrication of Copper-based Nanowires

1-dimensional metal nanostructures have gained considerable attention due to the unique properties, such as optical, mechanical, and electrical properties. Among many 1-D metal nanostructures, copper has gained attention due to low cost compared to silver and gold. Copper 1-D nanostructures, copper nanowire, displays high electrical/thermal conductivity, ductility, and malleability, further utilized in transparent

conducting electrode, solar cells, and catalysis. However, due to the oxidation, poor dispersibility, and stability, synthesis of copper nanowire requires precisely controlled methods. Oxidation becomes severe when size of the copper is reduced to nanoscale. Therefore, stabilization of copper nanowire during fabrication process still remains as complicated issues. [18-21]

Synthesis of copper nanowire includes precise control of nano-crystal growth. Copper ions are reduced using reducing agent to obtain nuclei, which acts as seed for the nano-crystal growth. Usually, the Ostwald ripening process leads the seed to grow to nanostructures. In most cases, seeds are created fast by nucleation, followed by slow growth process. There are several methods to fabricate copper nanowire which are previously reported before. Among the reported synthesis methods, solution phase synthesis is the most renowned method for facile fabrication process. The reaction temperature, time, rate, and capping ligands could affect the resultant nanostructures. Among many parameters, capping ligands play the key role in governing the growth of copper nanowires. Capping agents prevents coalescence and aggregation through stabilization. Also, it could affect the thermodynamic/kinetic

growth, leading to controlled morphology. The solution phase synthesis using capping agents and surfactants could be divided into several methods; wet chemical method, solvo-thermal method, microwave assisted method, and micro-emulsion method. [22]

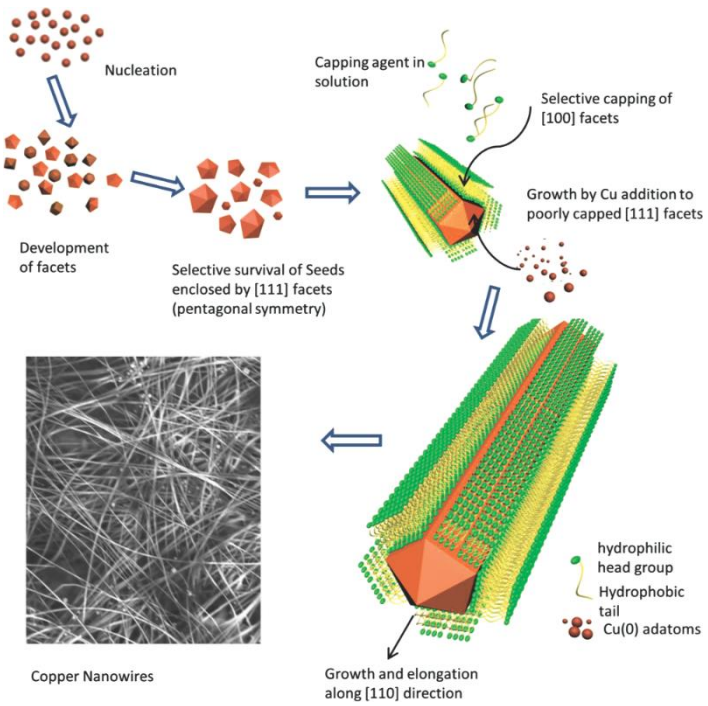

Figure 2. Schematic image of fabricating 1-D Cu nanostructures[22]

1.1.1.2.1. Wet chemical method

Wet chemical method is used to directly fabricate copper nanowire by reducing the copper ions. This method is favored in that it could aim for large scale fabrication even in mild reaction conditions. Hydrazine or oleylamine could be used as reducing agents, and EDA, HDA, and ODA as capping agents. Hua et al. synthesized 100 nm thick ultra-long copper nanowires using Cu-ethylenediamine as precursor at mil temperature of 60°C.[23] Also, Xia et al. fabricated high purity copper nanowires using hexadecylamine as the capping agent and hydrazine as the reducing agent.[24]

1.1.1.2.2. Solvo-thermal method

Copper nanowire could also be fabricated by solvo-thermal method which utilizes the high temperature and pressure conditions, and is also called hydrothermal method. Weak reducing agents could be utilized in solvo-thermal method as high pressure and temperature is used in the synthesis. Yitai utilized Cu-glycerol complex as the precursor and sodium dodecyl benzosulfonate (SDBS) as the capping ligand, and reacted in autoclave for 20 hrs to fabricate 85 nm thick copper

nanowires.[25]

1.1.1.2.3. Microwave assisted method

Unlike conventional reactor, microwave could be used to fabricate the copper nanowire. Microwave is better than conventional heat source in that it could selectively heat the materials and requires little energy. Pan et al. synthesized 50 nm thick copper nanowire using microwave assisted method with ascorbic acid as reducing agent.[26]

1.1.1.2.4. Micro-emulsion method

Copper nanowires could be fabricated in solution phase using micro-emulsion as the soft template. Micro-emulsion occurs when two immiscible phase meet each other, using surfactants or emulsifiers. Micro-emulsion could readily dissolve into both water-like phase and oil-like phase. Also, it exhibits large interfacial area and low interfacial tension. Therefore, it could be utilized as nano-reactors for fabricating copper nanowires. The cavity of the micelles formed control the size and shape of the nanowires. Huh et al. synthesized 600 nm thick copper nanowire through reduction of copper-amine complex in aqueous-

nonpolar system.[27]

1.1.2. Application Fields

1.1.2.1. Nanomaterials-based Conductive ink/paste

In these days, printed electronics became one of the most promising application for fabrication of electronic devices. Especially, manufacturing flexible electronics proved attractive in that it could be applied to numerous practical application. Conventional electronic devices are fabricated using multi-stage methods, such as photolithography, electroless plating, and vacuum deposition. However, these methods require expensive equipment and high cost manufacturing process. Therefore, the printed electronics, which is cost-efficient and fast, are getting large attention. In these days, the printed electronics are used in the fields of printed circuit boards, RFID tags, thin film transistors, light emitting devices, solar cells, transparent electrodes, and flexible displays.[28-32]

Conductive ink is usually composed of conductive material, liquid base, and various additives (binder, defoamer, humectants, or surface tension modifiers). These components join together to optimize the

performance of conductive ink. Conductive materials could be nanoparticles, organometallic compound, or conducting polymers. Conductive materials should be selected regarding the conductivity, adhesion ability, transparency, or stability.[30, 33]

Especially, metal nanoparticles have drawn considerable attention due the modern wet chemical technology which enabled the large-scale production of nanoparticles. Typically, silver nanoparticles-based inks are widely utilized these days due to the high conductivity.[34-36]

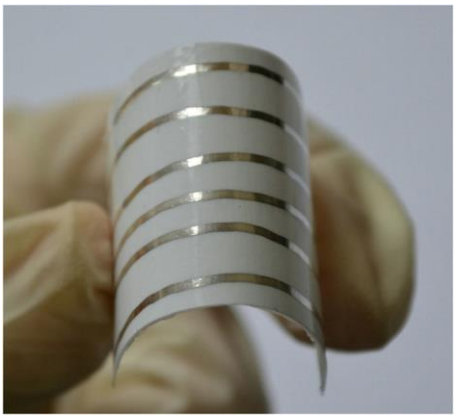

Figure 3. Silver nanoparticle-based conductive pattern drawn on paper substrate[37]

1.1.2.2. Dipole tag antenna

Dipole tag antenna is a wireless technique which enables large amounts of various information to travel across with low energy cost. At transmission stage, antenna receives electric current from the transmitter and convert it into electromagnetic waves. Then, at reception stage, antenna receives electromagnetic waves to convert it into electric current. Antennas could be designed to receive and sent radio signal from specific directions. Dipole tag antenna could be combined with the radio frequency identification (RFID) system to be used as RFID tag antenna. In the case of RFID antennas, omni-direction tag antenna is preferred in that it could receive identification from all directions.

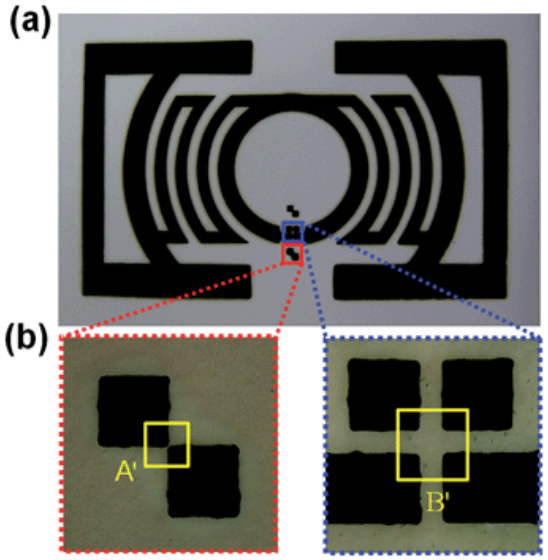

Figure 4. Pattern for dipole tag-antenna with optical image for enlarged section[38]

1.1.2.3. Glucose Sensor

Glucose sensing remains as one of the most important issue for researchers.[39] Therefore, glucose sensing system requires high stability, sensitivity, and selectivity to scrutinize the glucose level.[40-42] There are two kinds of glucose sensor; enzymatic glucose sensor and non-enzymatic glucose sensor. Enzymatic glucose sensor is sensitive to pH, humidity, temperature, reagents, etc. Therefore, non-enzymatic glucose sensor is favored in many ways in that it functions with direct oxidation of glucose on the electrode surface. There have been many researches on fabricating alternative to enzymes.[43, 44] Various nanomaterials were synthesized to be used in glucose sensors, such as noble metal, metal oxide, polymers, carbon materials, etc. Among the synthesized materials, metal nanomaterials have gained considerable attention for high sensitivity. Metal nanoparticles are favored in that they exhibit high surface area, high catalytic ability and high biocompatibility. High electroactive surface area of metal nanoparticles could demonstrate fast glucose detection and high sensitivity. Especially, copper has gained attention for its better catalytic activity, range of response, and excellent stability.[45]

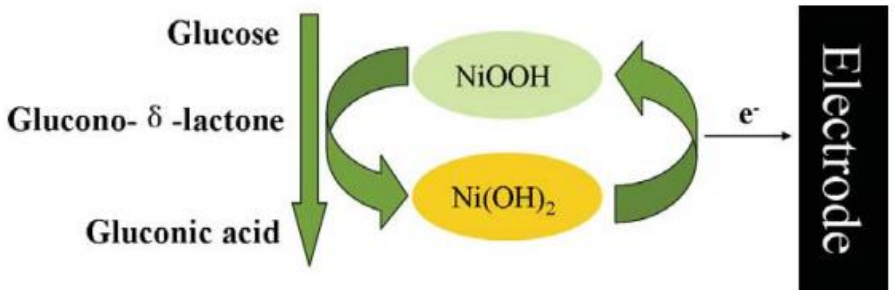

Figure 5. The working mechanism of Ni-based non-enzymatic glucose sensors[46]

1.2. Objectives and Outlines

1.2.1. Objectives

The aim of the dissertation is to provide fabrication methods of copper based nanomaterials, which could be utilized to various fields. Particularly, copolymer capped Cu nanoparticles and Cu nanowires were fabricated to be used in sinter-free conductive paste. These paste were further applied to other applications such as dipole tag antenna, and non-enzymatic glucose sensors.

1.2.2. Outlines

This dissertation focused on fabrication of copper based nanomaterials and applications to sinter-free conductive paste, dipole tag antenna, and non-enzymatic glucose sensors. This dissertation involves the following subtopics:

I. Fabrication of sinter-free Cu NW paste for non-enzyme glucose sensor

II. Fabrication of sinter-free conductive paste using sub-10 nm Cu NPs

III. Fabrication of sinter-free conductive paste using Cu NP and Cu NW

composite

A detailed outline of the story is as follows:

1. Cu NWs were fabricated using simple hydrothermal method. The traditional carbon pattern was substituted with highly conductive Cu NW paste for high sensing abilities. Fabricated Cu NW paste could be easily utilized without sintering due to the high conductivity of copper nanowires. Also, Cu NWs were used as the sensing material for detecting glucose. 1-Dimension of Cu NW grants high charge transport ability to the glucose sensor, leading to high sensing ability.

2. Sinter-free copper nanoparticle-based conductive paste (Cu NPs paste) were fabricated using simple method. The copper nanoparticles with the size below 10 nm enable the formation of integrated structure even without heat-treatment. Poly(vinylimidazole-co-vinyltrimethoxysilane) used in the synthesis grant the copper surface a high anti-oxidant ability over a temperature range up to 300 °C at ambient condition. Furthermore, the viscosity of the conductive paste could be arbitrarily adjusted while minimizing the change of the bulk resistance. The pattern printed using Cu NPs paste demonstrated

excellent electrical resistivity of $1.2 \cdot 10^{-2}$ Ω·cm for un-sintered conductive paste and retained electrical resistance in flexed state, indicating that Cu NPs paste could be applied in a wide variety of applications. The potential of the Cu NPs paste was confirmed through dipole tag antenna application.

3. Sinter-free Cu nanoparticle/Cu nanowire composite conductive paste (Cu NP/NW paste) was fabricated with simple method. Cu nanowire was mixed into Cu NPs paste to certain ratio to enhance conductivity and bending stability. The CP-Cu NPs made the paste conductive and Cu NWs grant the charge carrier to move fast within the conductive film. The Cu NP/NW paste with Cu NWs content of 20 wt% demonstrated best resistivity of $0.57 \cdot 10^{-2}$ Ω·cm. The further addition of Cu NWs led to decreased conductivity due to the increased number of large void arise from the large size of the Cu NWs. The potential of the Cu NP/NW paste was confirmed through the application of dipole tag antenna.

2. Experimental Details

2.1. Fabrication of Sinter-free Cu NW paste for non-enzyme glucose sensor

2.1.1. Fabrication of Cu NW

For typical synthesis, 0.12 g of glucose and 0.132 g of copper chloride were dissolved in distilled water (60 ml) and stirred for 15 min. Hexadecylamine were pre-heated to liquid state. 1 ml of hexadecylamine were added to the above solution and stirred for 12 hrs. Stirred solution were placed in autoclave and reacted at 120 °C for 24 hrs. The resulting solution were washed with water, hexane, and ethanol. The precipitate was dried in vacuum oven to obtain Cu NW powder.

2.1.2. Fabrication of Cu NWs based sinter-free conductive Cu paste (Cu NW paste) and Cu NW paste-based glucose sensor strip (Cu NW strip)

The paste was composed of Cu NWs, matrix polymer, and solvent. Ethyl cellulose (EC) and ethylene glycol butyl ether (EGBE) was utilized

as matrix polymer and solvent, each. EC was dissolved in the EGBE at 80℃ for 12 hr for mass ratio of 10, 20, and 25 % to make Base paste. Then, Cu NWs were mixed with the Base paste by mass ratio of 1:1 to fabricate Cu NW paste. Cu NW paste were printed on a glass substrate and dried at ambient condition for 3~4 hours to evaporate the solvent and used for characterization. Cu NW strip is fabricated by screen printing Cu NW paste and carbon paste on polyimide films, followed by printing Ag/AgCl paste on designated position. The paste was further dried for 4 hrs.

2.1.3. Characterization

Transmission electron microscopy (TEM), High resolution (HR)-TEM, and X-ray Photoemission spectroscopy (XPS) image were obtained using JEM-2100 (JEOL Ltd, Japan), JEM-3010 (JEOL Ltd, Japan), and SIGMA PROBE (VG, UK) installed at the National Center for Inter-university Research Facilities (NCIRF) at Seoul National University. X-ray diffraction (XRD) spectra were obtained using SMARTLAB. Electrical resistance was obtained using a Keithly 2400 source-meter with four-point probe. Cyclic voltammetry (CV) curves

2.2. Fabrication of Sinter-free Conductive Cu Paste using sub-10 nm Cu NPs

2.2.1. Fabrication Poly(VI-co-VTS) treated Cu NPs

Cu NPs were synthesized by using copper acetate monohydrate as precursor, and hydrazine monohydrate as reducing agent. For typical experiments, ethylene glycol (80 mL) and isopropanolamine (40 mL) were vigorously stirred together in ice bath. 4.0 g of copper acetate monohydrate were mixed with above solution and stirred for 15 min. Then, 10 mL of hydrazine monohydrate were rapidly injected into the above solution at 24 °C under vigorous stirring. The reaction remained for 18 hr. The resulting solution were precipitated using *N,N*-dimethylacetamide, followed by sequential washing using toluene and n-hexane. Precipitated Cu NPs were dried in vacuum oven at 60 °C. Synthesis procedure of poly(vinylimidazole-co-vinyltrimethoxysilane) is as follows. The monomer vinylimidazole (VI) and vinyltrimethoxysilane (VTS) were distilled in vacuum condition to yield pure and colorless liquid. Distilled liquid of VI and VTS was vigorously stirred before polymerization, followed by injection of

azobisisobutyronitrile (AIBN) solution to initiate the reaction. Concentration of monomer and initiator was fixed at 1 and 0.001 M each. The molar ratio of VI to VTS in the feed were adjusted to 15:1. The Poly(VI-co-VTS) was synthesized by polymerizing VI and VTS in isopropyl alcohol using free radical copolymerization, while stirred at 68°C under inert gas atmosphere. Solvent was removed from the resulting solution by rotary evaporator. Copolymer was precipitated using excess volume of ethyl ether. The Cu NPs were coated with poly(VI-co-VTS) as follows. The Cu NPs was added into a mixed solution of hydrochloric acid, phosphoric acid, distilled water and ethanol. Then, the mixture was sonicated and stirred with Poly(VI-Co-VTS) solution of ethanol. After stirred for 45 min, the mixture was washed with ether several times. Then the mixture was centrifuged and dried in vacuum oven.

2.2.2. Fabrication of Cu NPs based Sinter-free Conductive Cu Paste (Cu NPs paste)

The paste was composed of surface treated Cu NPs, matrix polymer, and solvent. Ethyl cellulose (EC) and ethylene glycol butyl ether (EGBE)

was utilized as matrix polymer and solvent, each. EC was dissolved in the EGBE at 80°C for 12 hr for mass ratio of 10, 20, and 25 % to make Base paste. Then, Cu NPs were mixed with the Base paste by mass ratio of 2:1 to fabricate Cu NPs paste. Cu NPs paste were printed on a glass substrate and dried at ambient condition for 3~4 hours to evaporate the solvent. The Cu NPs paste were printed in 100 μm to measure the bulk resistance. Antenna patterns were printed using screen printer with film thickness of 40 μm.

2.2.3. Characterization

Transmission electron microscopy (TEM), High resolution (HR)-TEM, and X-ray Photoemission spectroscopy (XPS) image were obtained using JEM-2100 (JEOL Ltd, Japan), JEM-3010 (JEOL Ltd, Japan), and SIGMA PROBE (VG, UK) installed at the National Center for Inter-university Research Facilities (NCIRF) at Seoul National University. FT-IR image was obtained using FT-IR Spectrometer (Frontier). The viscosity of Cu NPs paste were analyzed by using rheometer (AR2000 Advanced Rheometer, TA instruments). Thermogravimetric analysis (TGA) were done by using Pyris 6 TGA

(Perkin-Elmer). X-ray diffraction (XRD) spectra were obtained using SMARTLAB. Electrical resistance was obtained using a Keithly 2400 source-meter with four-point probe. E5071B ENA RF Network Analyzer from Agilent Technologies was used to characterize the RFID antennas.

2.3. Fabrication of sinter-free conductive Cu paste using Cu NP and Cu NW composite

2.3.1. Fabrication of Cu NW

For typical synthesis, 0.12 g of glucose and 0.132 g of copper chloride were dissolved in distilled water (60 ml) and stirred for 15 min. Hexadecylamine were pre-heated in liquid state. 1 ml of hexadecylamine were added to the above solution and stirred for 12 hrs. Stirred solution were placed in autoclave and reacted at 120 °C for 24 hrs. The resulting solution were washed with water, hexane, and ethanol. The precipitate was dried in vacuum oven to obtain Cu NW powder.

2.3.2. Fabrication of copper nanoparticles-based conductive paste (Cu NPs paste), copper nanowire-based conductive paste (Cu NWs

paste), and Copper nanoparticle and nanowire composite paste (Cu NP/NW paste)

All paste was composed of copper solid loadings, matrix polymer, and solvent. Ethyl cellulose (EC) and ethylene glycol butyl ether (EGBE) was utilized as matrix polymer and solvent, each. EC was dissolved in the EGBE at 80°C for 12 hr for mass ratio of 10, 20, and 25 % to make base paste. Then, copper solid loadings (CP-Cu NPs, Cu NWs) were mixed with the base paste by mass ratio of 2:1 to fabricate conductive paste. Cu NPs paste, Cu NWs paste, Cu NP/NW paste each used CP-Cu NPs, Cu NWs, and both for copper solid loadings. Copper conductive paste were printed on a glass substrate and dried at ambient condition for 3~4 hours to evaporate the solvent. The Cu NPs paste were printed with approximately 100 μm to measure the resistivity. Antenna patterns were printed using screen printer with film thickness of 40 μm.

2.3.3. Characterization

Transmission electron microscopy (TEM), High resolution (HR)-TEM, and X-ray Photoemission spectroscopy (XPS) image were obtained using JEM-2100 (JEOL Ltd, Japan), JEM-3010 (JEOL Ltd,

Japan), and SIGMA PROBE (VG, UK) installed at the National Center for Inter-university Research Facilities (NCIRF) at Seoul National University. FT-IR image was obtained using FT-IR Spectrometer (Frontier). The viscosity of Cu NPs paste were analyzed by using rheometer (AR2000 Advanced Rheometer, TA instruments). X-ray diffraction (XRD) spectra were obtained using SMARTLAB. Electrical resistance was obtained using a Keithly 2400 source-meter with four-point probe. E5071B ENA RF Network Analyzer from Agilent Technologies was used to characterize the RFID antennas.

3. Results and Discussion

3.1. Fabrication of Sinter-free Cu NW paste for non-enzyme glucose sensor

3.1.1. Fabrication and characterization of Cu NW

Figure 6 exhibits the schematic image of synthesis of Cu NWs. Cu NWs were fabricated using $CuCl_2$, HDA, and glucose as Cu precursor, capping agent, and reducing agent respectively. For the typical synthesis, $CuCl_2$ and glucose were dissolved in the distilled water with molar ratio of 1:2. Then, the solution was magnetically stirred for 10 min, followed by addition of 1 ml of HDA. HDA was melted into liquid state in the 60 °C oven prior to use. The solution was left to be stirred for 12 hrs. Stirred solution was moved to steel autoclave and reacted for 24 hrs at 120 °C. The resultant was washed with water, ethanol, and n-hexane to obtain fluffy red solid. The obtained Cu NWs were dried in vacuum oven and used for characterization.

HDA is used in the synthesis as capping agent. The (100) facets of the growing copper is selectively capped by HDA, which allows the Cu NWs

to grow in the direction of (111) facets, resulting in the fabrication of Cu NWs. **Figure 7a and b** illustrate the TEM and SEM image of fabricated Cu NWs. It is confirmed that Cu NWs were fabricated with average diameter of 80 nm. Also, High resolution transmission electron microscopy (HR-TEM) images and fast fourier transform (FFT) spectra were obtained to further analyze the fabricated Cu NWs. **Figure 7c** exhibits that lattice fringes are clearly formed within the Cu NWs. Furthermore, the diffraction from the (200) and (111) planes of fcc copper is clearly visible from the FFT spectra of the Cu NWs (**Figure 7d**).

To scrutinize the lattice structure of the synthesized Cu NWs, XRD spectra was obtained (**Figure 8**). The sharp peak at 2θ of 43.5, 50.7, and 74.4° each refers to (111), (200), and (220) planes of face centered cubic (fcc) structure of Cu, which corresponds with the lattice structure of the FFT spectra.[6] Therefore, it can be concluded that Cu NW is well composed of pure Cu. However, the small peak around 36.5 refers to the small amount of Cu_2O. Small amount of oxide might have formed while Cu NWs were dried in vacuum oven for XRD measurement.

Cu NWs were fabricated to substitute the traditional carbon conductive paste used in the sensor pattern, which exhibit high resistivity. Replacing the carbon paste with highly conductive paste could increase the sensitivity, which enables the sensor to detect even the small amount of target materials. Therefore, Cu NW based conductive paste was fabricated to replace the intrinsically low-conductive carbon materials for sensor pattern.

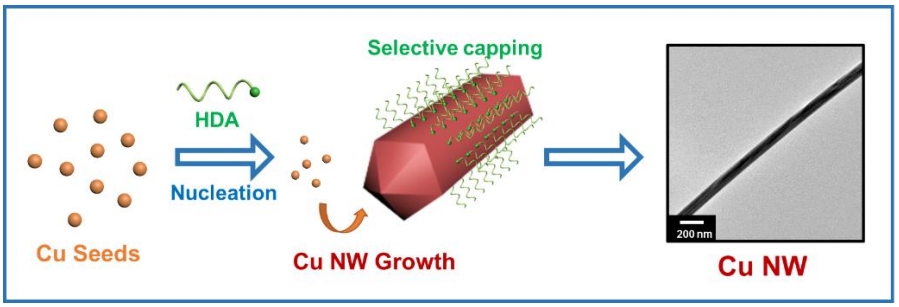

Figure 6. Schematic image of fabricating Cu NWs

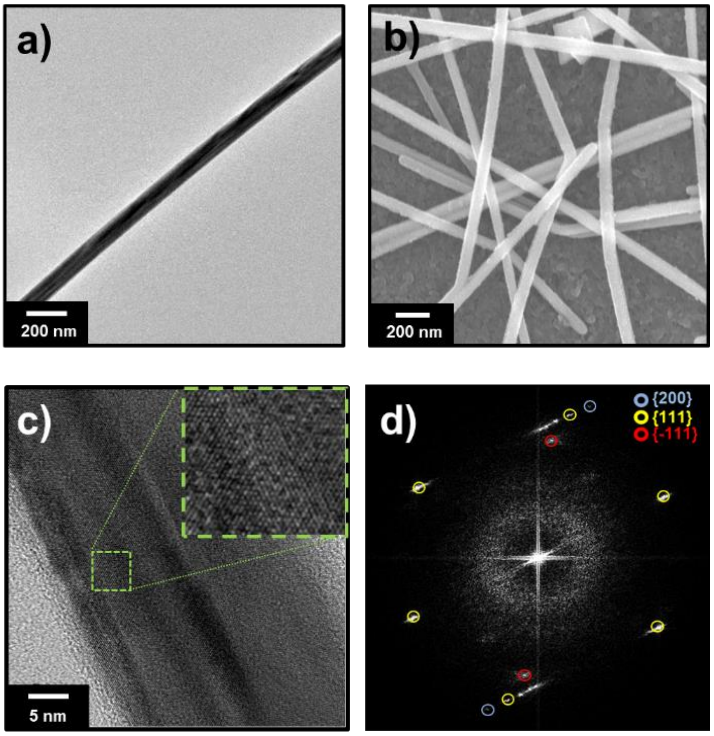

Figure 7. a) TEM, **b)** SEM, **c)** HR-TEM, and **d)** FFT image of synthesized Cu NWs

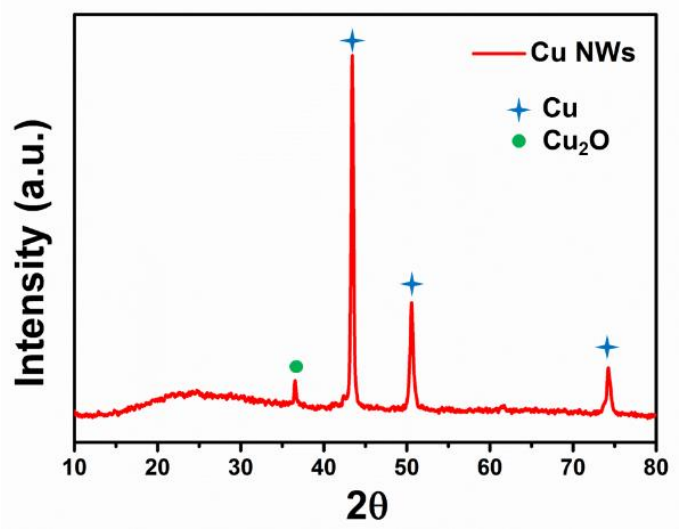

Figure 8. XRD spectra of fabricated Cu NWs

3.1.2. Fabrication and characterization of Cu NW Paste

The Cu NW paste was fabricated by following method. First, 'Base paste' was made by mixing ethyl cellulose (EC) and ethylene glycol butyl ether (EGBE) with weight ratio of 1:4. EC and EGBE is used as binder and solvent in the paste. Then, the base paste is mixed with pre-synthesized Cu NWs with weight ratio of 1:1 to obtain Cu NW paste. The fabricated paste is printed on the desired substrate and dried in ambient condition for 4 hrs. Another advantage of using Cu NW paste is that it does not require additional heat sintering to grant the conductivity to the printed film. In case of carbon paste pattern, it does not bare conductivity unless it is applied with heat. **Table 1** shows the resisitivity of the conventional carbon paste and fabricated Cu NW paste. Both paste were printed on a glass substrate for the measurement of resistivity. Carbon paste were sintered at 120 °C for 30 min. However, Cu NW paste were left at ambient temperature for 4 hrs before the measurement. The resistivity of Cu NW paste was 35.8 mΩ cm, which was 2.8 times lower than that of commercial carbon paste (97.1 mΩ cm). It could be confirmed that Cu NW paste shows lower resistivity than the carbon paste even though it was not applied with thermal sintering.

For the detailed analysis, SEM images of surface of the Cu NW paste were obtained (**Figure 9**). It could be confirmed that Cu NWs are tangled up together to form the charge transfer route. Even though lots of void exists within the conductive film, Cu NWs are overlapped together to grant the passage way for the electron. Also, to confirm that pure copper is still intact after Cu NW is made into Cu NW paste, XRD spectra was obtained (**Figure 10**). XRD spectra displays clear peak at 2θ of 43.5, 50.7, and 74.4°, which corresponds with the fcc structure of copper. Therefore, it can be concluded that Cu NW paste is successfully fabricated.

Table 1. Thickness and resistivity of conventional carbon paste and fabricated Cu NW Paste

	Thickness (μm)	**Resistivity (Ω·cm)**
Carbon Paste	75	$9.71 \cdot 10^{-2}$
Cu NW Paste	104	$3.58 \cdot 10^{-2}$

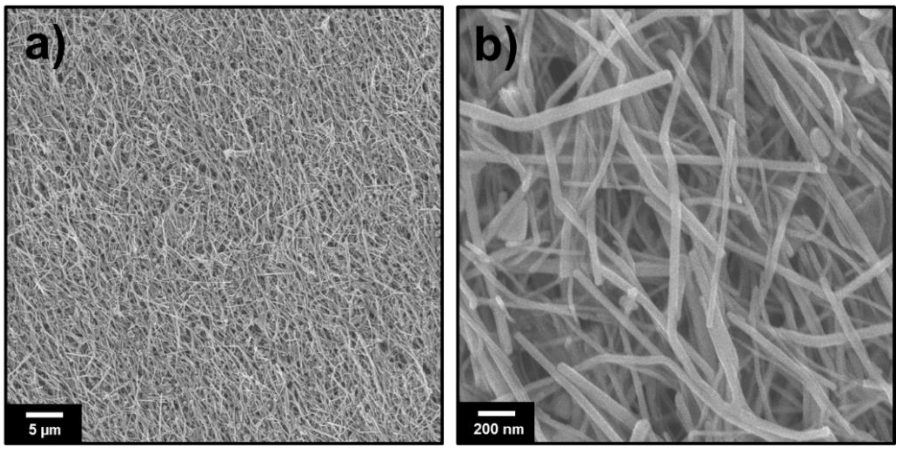

Figure 9. SEM images of surface of the Cu NW paste; magnification scale; **a)** 1:2000, **b)** 1:20000

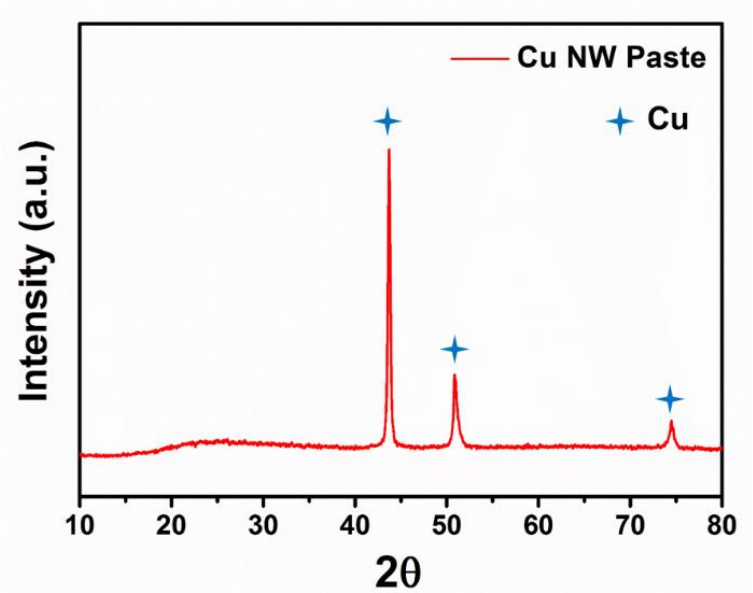

Figure 10. XRD spectra of printed pattern of Cu NW paste

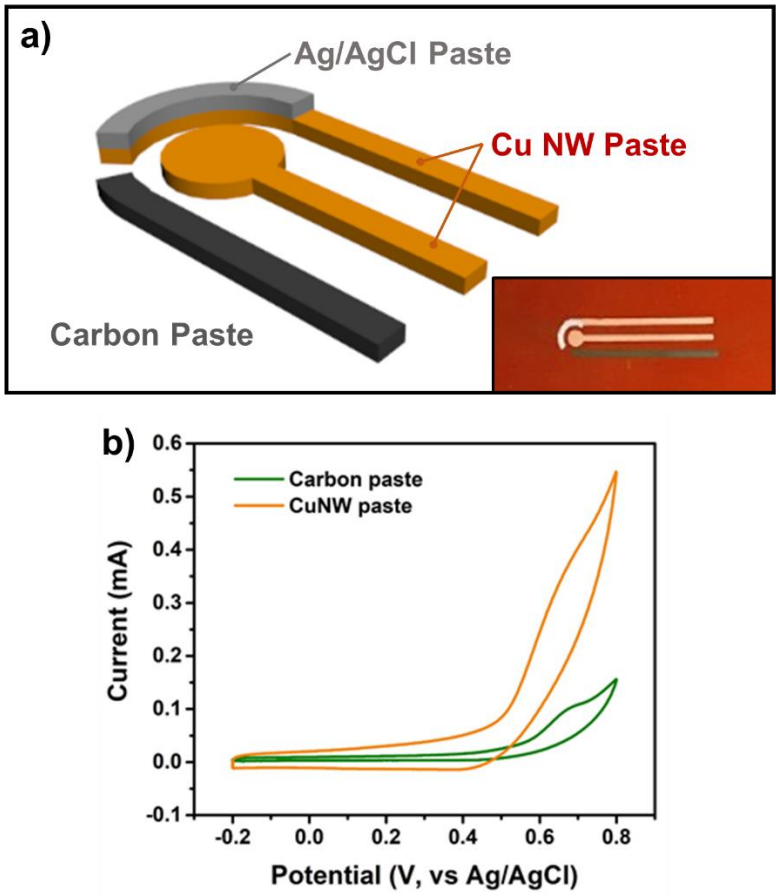

Figure 11. a) Schematic image of fabricated Cu NW strip (inset : photo of Cu NW paste sensor strip) and **b)** Cyclic voltammetry curves of carbon paste sensor strip and Cu NW strip in 0.1 M NaOH solution (scan rate: 50 mV s^{-1})

3.1.3. Fabrication and characterization of Cu NW strip

To compare the performance of Cu NW paste with commercial carbon paste, the electrochemical analysis and conductivity comparison were demonstrated. **Figure 11a** illustrates the schematic image of the fabricated Cu NW paste glucose sensor strip (Cu NW strip). The carbon paste and Ag/AgCl paste were used us counter electrode and reference electrode respectively. The Cu NW paste is employed in the Cu NW strip as both conductive electrode and glucose sensing materials. **Figure 11b** displayed the cyclic voltammetry (CV) curves of Cu NW strip and carbon paste sensor strip. The current significantly increased when Cu NW paste is used as working electrode. For these reasons, the Cu NW paste is absolutely alternative materials for conductive paste.

The electrochemical activities of the Cu NWs were studied by CV at various scan rates with 0.1 M KCl and 5 mM potassium ferricyanide as supporting electrolyte. **Figure 12** exhibits two pairs of well-defined redox peaks of Cu NWs. They displayed quasi-reversible electron transfer behavior with peak separations (ΔE_p) of *ca*. 0.19 and 0.65 V (vs. Ag/AgCl) for Cu NWs at a scan rate of 50 mV s^{-1}. These means that the Cu NWs have two redox reactions during electrochemical analysis. For

the glucose detection, the anodic and cathodic redox peaks around 0.6 V are related for sensor strip.[47]

The performance of Cu NW strip was demonstrated by monitoring electrochemical sensing results of CV curves and amperometric current responses. **Figure 13a** displays the CV curves of Cu NW strip in 0.1 M NaOH solution with various glucose concentrations from 1 nM to 100 mM at scan rate 50 mV s^{-1}. As the concentration of glucose increased, the anodic current increased, whereas the cathodic current decreased. These observations typically indicate that the main sensing mechanism of glucose is an irreversible electro-oxidation process, which could be described with the following reactions.[48]

$Cu + 2OH^- \rightarrow Cu(OH)_2 + 2e^-$

$Cu(OH)_2 + OH^- \rightarrow CuOOH + H_2O + e^-$

$CuOOH + e^- + glucose \rightarrow CuO + OH^- + gluconolactone$

$gluconolactone + Cu^{2+} \rightarrow gluconic\ acid\ (hydrolysis) + Cu^{2+}$

The Cu(II)/Cu(III) redox couple plays a critical role for nonenzymatic glucose sensing. The Cu(0) is electrochemically oxidated to Cu(II) at the

negative potential and further oxidated to Cu(III) at the potential around 0.65 V. After the addition of glucose, electrons are rapidly transferred from glucose to the Cu NW electrodes. During the cycling, a Cu(III) ion receives electrons and acts as an electron delivery carrier, generating the anodic signal.[49]

The CV curves of Cu NW strip in 0.1 M NaOH solution with 10 μM of glucose at various scan rates from 10 to 200 mV s^{-1}, as presented in **Figure 13b**. The anodic and cathodic current slightly shifted negatively and positively, respectively, which indicate that the electro-oxidation of glucose on the Cu NWs electrode is a diffusion-controlled process. Furthermore, the steady-state amperometric measurement was carried out on the basis of the CV analysis (**Figure 13c**). The biased potential was 0.65 V, which is major anodic peak at CV curve (scan rate: 50 mV s^{-1}). During the test, the certain amount of increasing concentration of glucose was successively injected into the 0.1 M NaOH solution, which immediately induced the current to leap. However, Cu NW strip didn't exhibit rapid response to steady-state due to the interference of ethyl cellulose polymer in the Cu NW paste. Nevertheless, due to its good conductivity, the Cu NW strip displayed higher sensitivity toward

glucose (1 nM) than other sensors, as illustrated in **Table 2**. This limit of detection (LOD) is enough to detect glucose in human saliva, which is promoting technique of diagnosing diabetes with noninvasive method (not using blood). **Figure 13d** displays the calibration plot of real-time response of Cu NW strip. The plot demonstrated the higher current changes as the concentration of glucose increases. The saturation appeared at 100 μM, which is 10^5 times higher concentration of LOD.

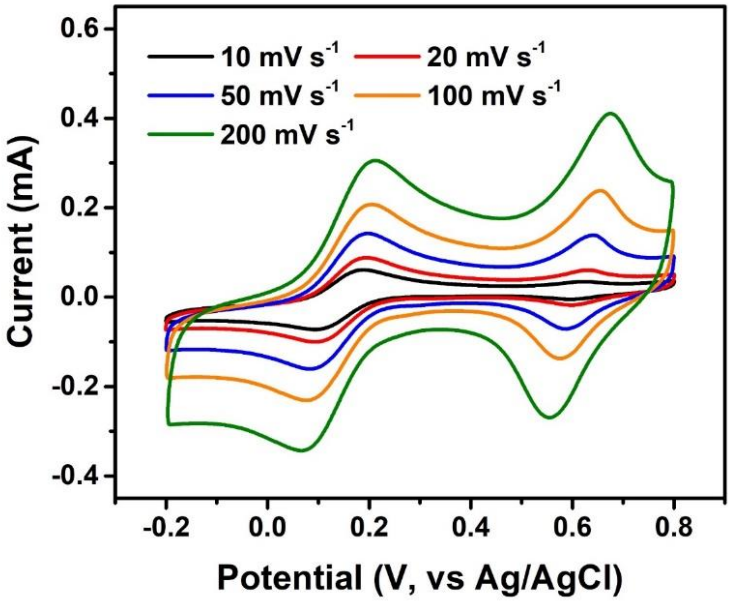

Figure 12. CV curves of CuNW paste sensor strip in 0.1 M KCl and 5 mM $K_3[Fe(CN)_6]$ with various scan rates from 10 to 200 mV s^{-1}.

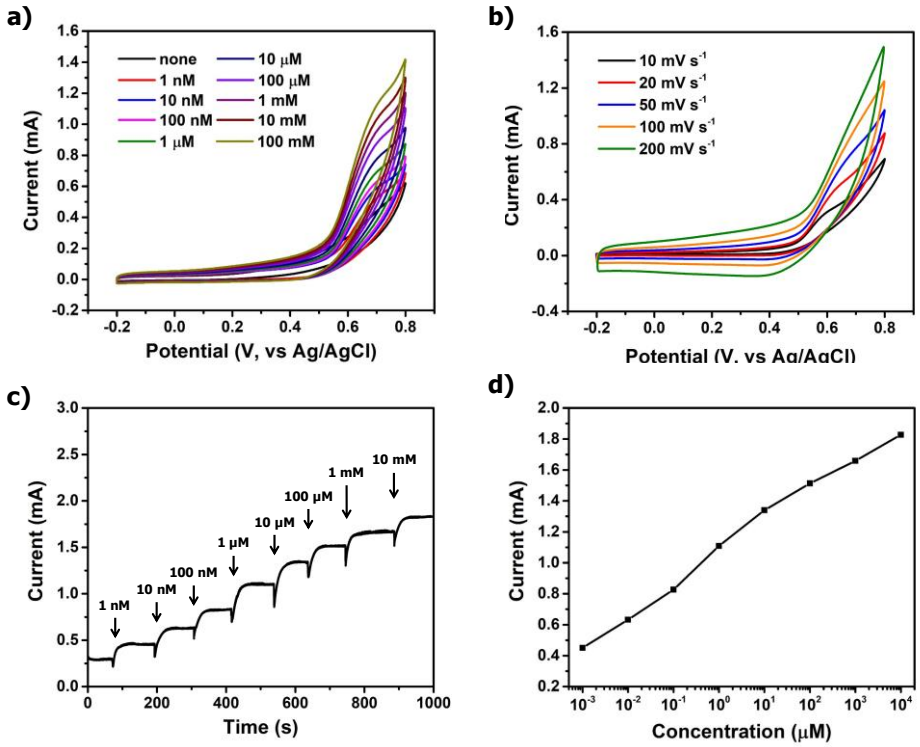

Figure 13. **a)** CV curves of Cu NW strip in 0.1 M NaOH solution with various glucose concentrations from 1 nM to 100 mM (scan rate: 50 mV s^{-1}). **b)** CV curves of Cu NW strip in 0.1 M NaOH solution with 10 μM of glucose at various scan rates from 10 to 200 mV s^{-1}. **c)** Amperometric responses of Cu NW strip on the successive injection of different concentration of glucose in 0.1 M NaOH solution (applied potential: 0.65 V). **d)** Calibration plot of amperometric current response as a function of different concentration of glucose.

Table 2. Performance comparison of various non-enzymatic glucose sensors based on Cu nanomaterials.

Electrode materials	**Limit of detection (nM)**	**reference**
CuNPs/GO/SWCNTs	340	[48]
CuNWs/rGO	200	[49]
CuNPs/PEDOT	47	[50]
CuNPs/rGO	3400	[51]
CuNWs	35	[52]
Cu foam	980	[53]
CuNPs/MWCNTs	2000	[54]
CuNWs/MWCNTs	260	[55]
CuNPs/graphene	1300	[56]
Cu/Carbon NWs	50	[57]
CuNW paste	1	This work

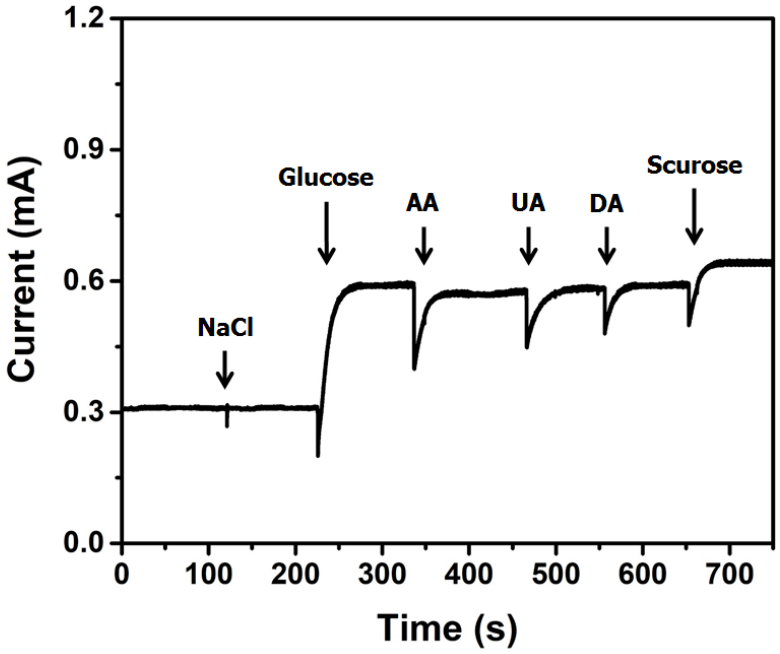

Figure 14. Amperometric selectivity response of Cu NW strip toward non-target (0.1 M NaCl, 10 μM ascorbic acid (AA), 10 μM Uric acid (UA), 10 μM dopamine (DA), 10 μM sucrose) and target (glucose) analytes (applied potential: 0.65 V).

The selectivity test was proceeded to explore the application to reliable platform for glucose sensor strip. The interfering non-target species usually exist with glucose in real blood serum and similar carbohydrate (AA, UA, DA, and Sucrose) was used to determine the selectivity of the Cu NW strip. As illustrated in **Figure 14**, no meaningful signal was detected without glucose. Moreover, chloride ion, which cause some poisoning and degrading metal-based non-enzymatic glucose sensor, also displayed no significant signal at the selectivity test. Therefore, it can be confirmed that Cu NW strip possess high detecting selectivity to glucose.

3.2. Fabrication of Sinter-free Conductive Cu Paste using sub-10 nm Cu NPs

3.2.1. Fabrication of Cu NPs Paste

Figure 15a illustrates the synthetic procedure of copper nanoparticles (Cu NPs). Amine was used for capping the nanoparticles to regulate the size and protect the copper from corrosion at the same time. Especially, isopropanolamine (IPA) was used in the synthesis in that it contains both hydroxyl groups and amino groups, which could bind more strongly to the copper surface for enhanced stability.[58, 59] Firstly, ethylene glycol and IPA were mixed together in ice-cold bath. Then, copper acetate monohydrates, copper precursor, were added into the above solution. Introducing the copper precursor at low temperature could prevent the precursor from being reduced to copper prior to adding the reducing agents. Hydrazine monohydrates, reducing agent, were rapidly injected into the above solution at room temperature of 24 °C. Fast injection rates and strong reducing capabilities of hydrazine allows the fabrication of copper nanoparticles with smaller size.[58, 60] Reactions were maintained for 18 hrs with vigorous stirring after the injection of reducing agent to

ensure complete formation of Cu NPs. TEM and HR-TEM images were obtained to confirm that the Cu NPs were successfully prepared (**Figure 15b and c**). Fabricated copper nanoparticles were highly dispersed and showed sizes lower than 10 nm. **Figure 15c** displays magnified image of copper nanoparticles with lattice fringes of 0.2 nm, which corresponds with the (111) plane of face-centered cubic (fcc) structures of copper.[61]

Figure 16a represents the manufacturing process of Poly(VI-co-VTS). The synthesized copolymers play a key–role in imparting additional thermal stability and antioxidant capabilities to Cu NPs. Poly(VI-co-VTS) were fabricated by mixing VI and VTS at a specific ratio with isopropyl alcohol as solvent. Nitrogen in the imidazole ring and silane groups in the VTS interact with copper surface, allowing the copolymer to better interact with the copper surface. The nitrogen in the imidazole ring possess lone pair electron, which could create charge transfer complex to electrostatically binds the copolymer to the copper. Silane groups are hydrolyzed to form covalent bond, Si-O-Cu with the copper surface.[62-65] Moreover, imidazole group possess the ability the withstand high temperatures itself, making poly(VI-co-VTS) thermally stable. AIBN was added to the above solution to initiate the free radical

copolymerization of both monomers. Then, solvent was evaporated from the resultant solution using a rotary evaporator, and copolymers were obtained by precipitation method using excess volume of ethyl ether.

To further identify the synthesized poly(VI-co-VTS), Fourier transform infrared (FT-IR) spectrum of the copolymer was obtained and presented in **Figure 16b**. Characteristic peaks of imidazole ring and trimethoxysilane groups are clearly visible in the FT-IR spectra. The peak at 3100 cm^{-1} represents stretching of C=C-H and N=C-H in the imidazole ring, and the two peak at 1650 and 1495 cm^{-1} refers to stretching of C=N and C=C. Moreover, the two peaks at 1226 and 1284 cm^{-1} originates from the vibration of the imidazole rings, which indicates the presence of imidazole group in the synthesized copolymer. The peaks originated from the trimethoxysilane groups are as follows. The two peaks around 2800 ~ 3000 cm^{-1} represents CH_3 stretching derived from Si-O-CH_3, and two peaks at 816, 1080 cm^{-1} indicates Si-O-C stretching. Through detailed observation, it can be concluded that the copolymer, poly(VI-co-VTS), was well fabricated.

The synthesized poly(VI-co-VTS) was used to treat the surface of the Cu NPs as described in **Figure 19a**. Firstly, Cu NPs were dispersed in

water and ethanol using sonication method, followed by the addition of small amount of hydrochloric acid and phosphoric acid. Added acids removes the partially oxidized copper on the particle surface and temporarily passivate the copper surface, so that copolymers could be well treated on the pure copper. Poly(VI-co-VTS), which was dissolved in the ethanol, was introduced in the above solution and stirred for 45 min at room temperature to obtain copolymer treated copper nanoparticles (CP-Cu NPs).

To scrutinize the properties of Cu NPs and CP-Cu NPs, X-ray photoelectron spectroscopy (XPS) spectra were obtained for both particles. **Figure 17** displays XPS spectra of Cu NPs and CP-Cu NPs for the Cu2p and N1s signals. **Figure 17a** depicts the deconvoluted XPS spectra of Cu 2p signal. Peaks at 932.7, 934.5, and 936.0 eV indicates the presence metal copper, copper oxide (CuO), and $Cu(OH)_2/CuCO_3$ respectively.[66, 67] Both Cu NPs and CP-Cu NPs displayed small peaks of copper oxide and $Cu(OH)_2/CuCO_3$, which is likely due to the slight oxidation of particle surface. N1s signal of Cu NPs and CP-Cu NPs are illustrated in **Figure 17b**. N1s signal for Cu NPs shows clear peak at 399.7 eV, which indicates the presence of IPA capping the surface of Cu

NPs. Deconvoluted N1s signal for CP-Cu NPs displays two peaks at 399.6 and 401.0 eV, which both refers to the N atoms in imidazole ring, pyridine-like N in the outer side of the ring and pyrrolic N.[68, 69] As a result, it is confirmed that CP-Cu NPs were well treated with poly(VI-co-VTS).

Thermogravimetric analysis (TGA) on Cu NPs and CP-Cu NPs was conducted to confirm that fabricated copolymers could prevent the oxidation of Cu NPs even at high temperatures (**Figure 18**). Cu NPs not treated with copolymers began to gain weight as soon as the temperature rose above 100 °C due to the oxidation of copper. However, the mass of CP-Cu NPs did not increase until the temperature reaches 400 °C. Slight reduction in mass through 100 to 300 °C indicates loss of water residues and silane groups in the copolymer. The copolymers began to decompose over 300 °C and mass began to rise above 400 °C due to oxidation of copper. Therefore, it is concluded that CP-Cu NPs could withstand temperatures as high as 300 °C under ambient condition without oxidation.

Figure 19a depicts the overall synthesis procedure of Cu NPs paste. Cu NPs paste was made by mixing ethyl cellulose (EC), ethylene glycol

butyl ether (EGBE), and CP-Cu NPs for certain ratio. EC and EGBE act as matrix polymer and solvent respectively. The mixing ratio of EC and EGBE could be adjusted to variate the features of Cu NPs paste. Therefore, the mixing ratio of EC is adjusted to 10, 20, and 25 % by weight to control the viscosity of the copper paste, so that it could be utilized to various application fields with ease.

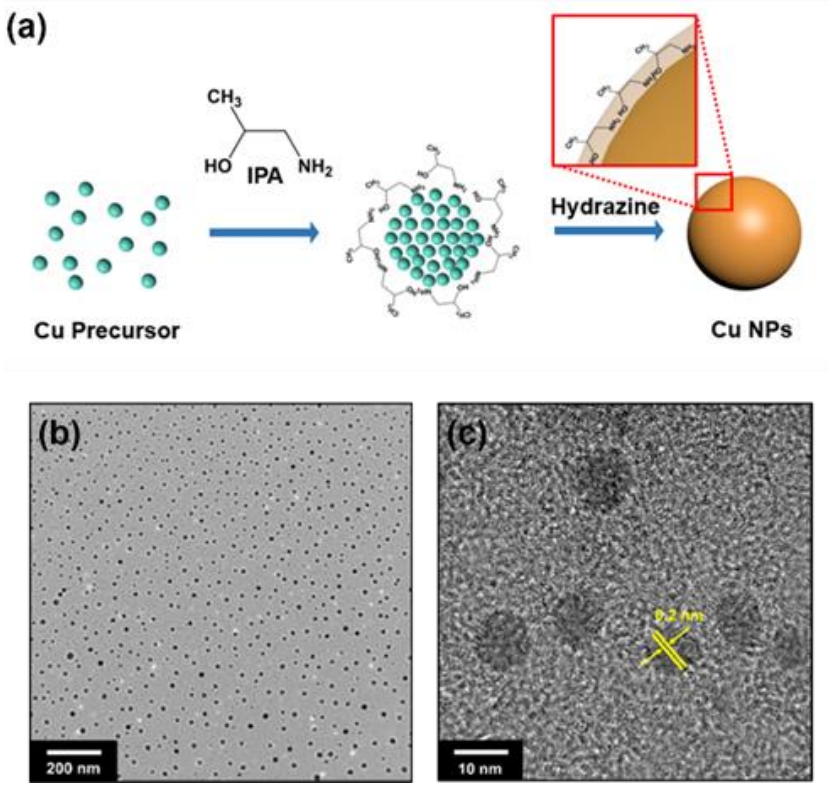

Figure 15. **a)** Schematic image of synthesis procedure and **b)** TEM and **c)** HR-TEM image of Cu NPs

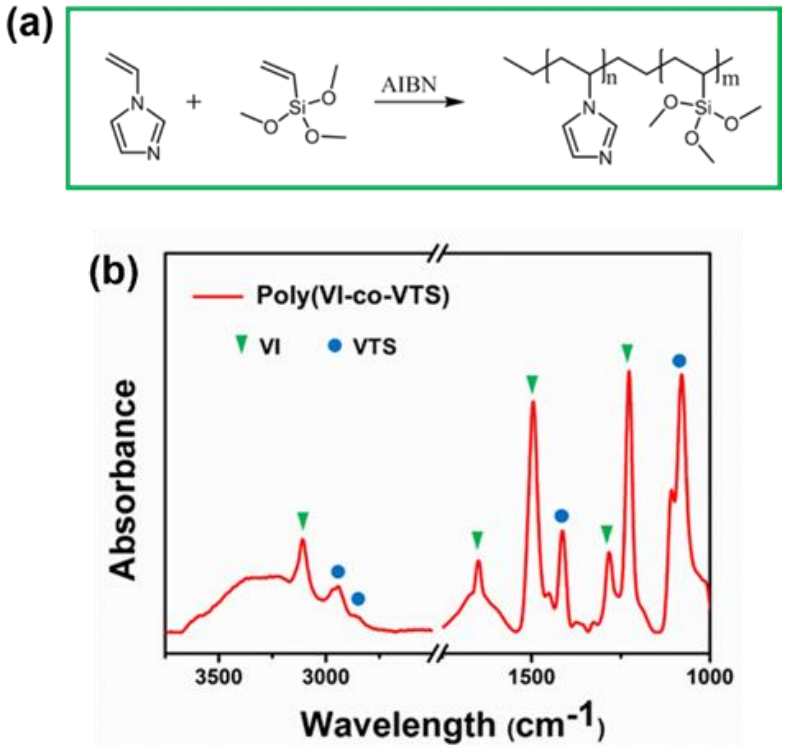

Figure 16. a) Fabrication procedure and **b)** FT-IR image of Poly(VI-co-VTS)

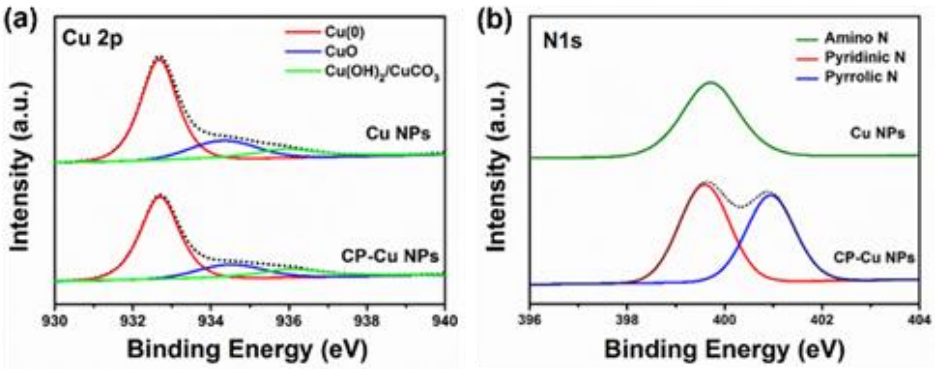

Figure 17. XPS spectra of Cu NPs and CP-Cu NPs for **a)** Cu2p and **b)** N1s signal

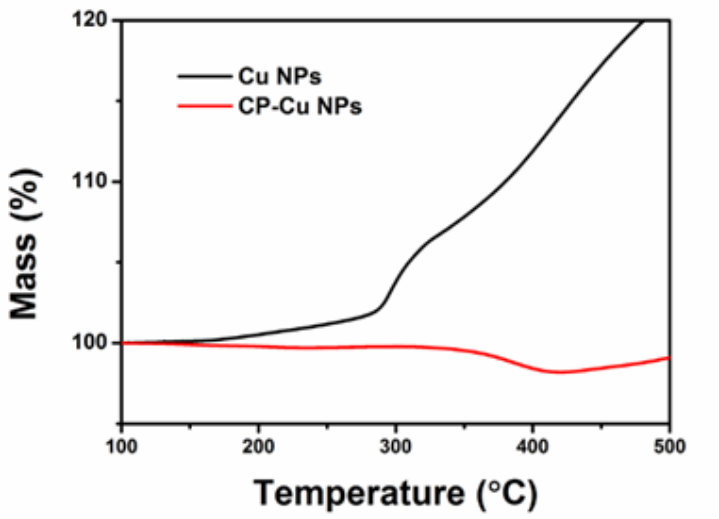

Figure 18. TGA analysis of Cu NPs and CP-Cu NPs

3.2.2. Characterization of Cu NPs Paste

To further investigate the fabricated Cu NPs paste, X-ray diffraction (XRD) patterns of Cu NPs, CP-Cu NPs, and Cu NPs paste with different viscosities was obtained (**Figure 19b and c**). All the spectra displayed sharp diffraction peaks around 2θ angles of 43.6, 50.8, and 74.4°, each refers to (1,1,1), (2,0,0), and (2,2,0) crystal planes of face-centered cubic.[6] The three types of Cu NPs paste exhibit broad peaks near 2θ angles of 20° to 30°, corresponding to the EC used in the synthesis process. It is observed that the diffraction peaks of the metallic copper remain intact even after Cu NPs were treated with copolymer and made into Cu NPs paste. Therefore, it can be confirmed that inherent features of the copper nanoparticle well remain even after they are made into conductive paste.

Since low viscosity of conductive paste make many applications difficult, I focused on making the viscosity of Cu NPs paste high enough. In particular, the viscosity of the conductive paste is required to be 500 to 50,000 mPa·s for screen printing.[70] Therefore, the viscosity of the Cu NPs paste was adjusted sufficiently high enough so that it could be easily used for screen printing method. Viscosity data for each Cu NPs

paste was obtained for further analysis of the Cu NPs paste. **Figure 20b, c, and d** exhibit the plots of viscosities of Cu NPs paste with different EC content by shear rate. All Cu NPs paste exhibited the shear-thinning behaviour; viscosity decreased with the increased shear rate.[71] This phenomenon is attributed to the disentanglement and re-orientation of polymer chains in the direction of shear flow as the shear rate increases.[72],[73] Overall viscosity increases with higher EC content as the matrix polymer increases viscosity. Furthermore, capability to create variety of viscosities as desired allows Cu NPs to be used for various applications, such as pen or spin-coating method.

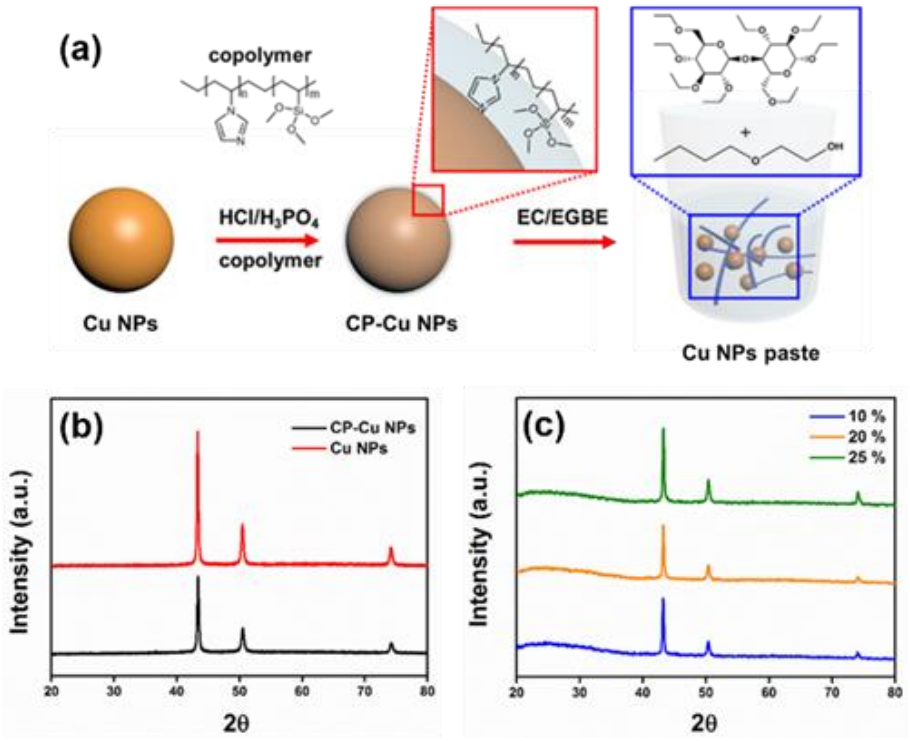

Figure 19. a) Synthesis procedure of Cu NPs paste and XRD spectra of **b)** Cu NPs, CP-Cu NPs and **c)** 3 kinds of Cu NPs paste of different viscosities

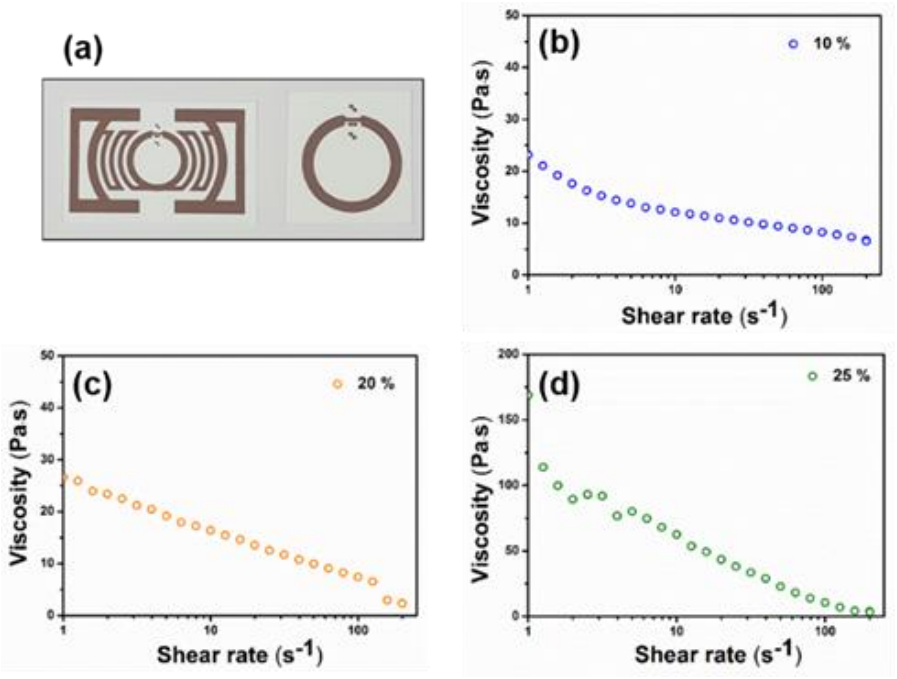

Figure 20. a) Screen printed patterns of Cu NPs Paste and plots of viscosity as a function of shear rate for Cu NPs paste with EC content by **b)** 10, **c)** 20, and **d)** 25 %.

Table 3. Thickness and resistivity of sinter-free conductive paste made of bulk copper, Cu NW, and Cu NP

	Thickness (μm)	**Resistivity (Ω·cm)**
Bulk Cu	40	3.19
Cu NW paste	140	$3.58 \cdot 10^{-2}$
Cu NP paste	120	$1.21 \cdot 10^{-2}$

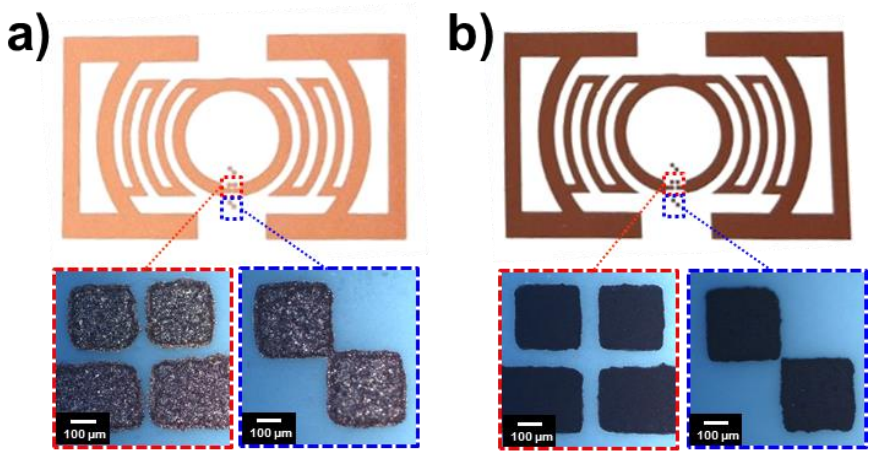

Figure 21. Pattern for dipole tag-antenna with optical image for enlarged section using **a)** bulk-copper paste and **b)** Cu NP paste

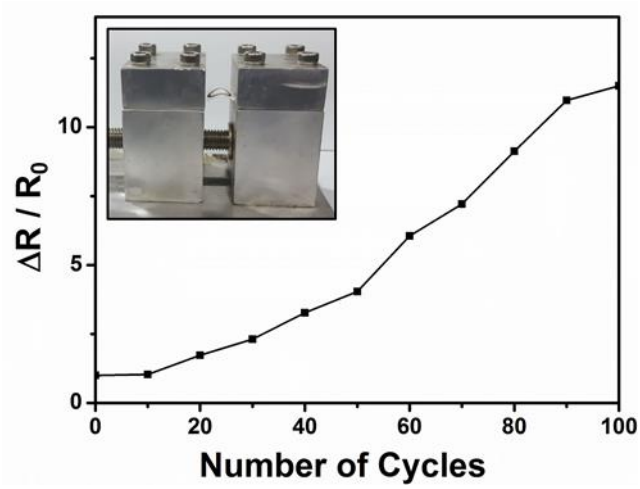

Figure 22. Bulk resistance changes of printed pattern of Cu NPs paste as a function of number of cycles that film was bent (bending radius = 15 mm)

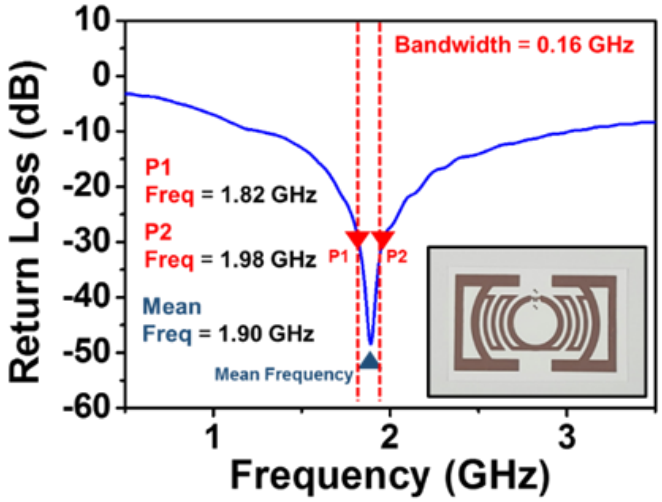

Fig 23. Return loss curve of the dipole tag antenna using Cu NPs Paste-based electrode (inset: Printed antenna pattern using Cu NPs Paste)

3.2.3. Performance of Cu NPs Paste

Bulk resistance of the fabricated copper paste was measured to confirm the availability for application. The Cu NPs paste with EC content of 10, 20, and 25 % displayed average electrical resistance of 1.07, 1.21, and 1.42 Ω respectively, and showed no significant change according to viscosity. The Cu NP paste with EC content of 10wt% presented resistivity of $1.21 \cdot 10^{-2}$ Ω·cm, which is almost 264 times lower than that made of bulk copper (3.19 Ω·cm). The reason Cu NPs paste exhibit higher conductivity than bulk copper paste and Cu NW paste even without heat-treatment is attributed to the small size of copper nanoparticles (**Table 3**). The metal particles with smaller size could form a conductive network through the metal-polymer complex more easily.[74] Small particles could gather together to form indiscrete structure with minimal void, while large particles require additional heat treatment to form coalescence for high conductivity. Therefore, most researches on fabrication of copper nanoparticle-based paste requires heat treatment for high conductivity. Basically, printed patterns are sintered for 100 to 300 °C in inert condition in order to remove solvents and induce coalescence between the copper nanostructures.[75]

However, many polymer and organic substrates could not withstand such high temperature sintering, especially in ambient air. Therefore, copper nanoparticles-based copper paste that exhibit excellent conductivity without heat treatment could be a breakthrough invention in many applications, such as solar cells and sensors. Moreover, Cu NP paste could be printed with more clear line patterning compared to bulk Cu paste, which makes it more reliable to be used for various applications (**Figure 21**). In addition, electrical fatigue test was performed to verify that the electrical resistance of the Cu NPs paste remains undamaged by external forces (**Figure 22).** The cycling test of printed pattern of Cu NPs paste were held. The printed pattern retains almost same resistance until bent for 100 times with bending radius of 15 mm. Therefore, it can be concluded that Cu NPs paste maintains good conductivity after severe bending and possess potential for application to flexible substrate.

In order to confirm the performance of copper paste for actual application, Cu NP paste were employed for dipole tag antenna pattern. The antenna pattern was prepared on a flexible substrate using the screen printing method for film thickness of 40 μm. The inset image in **Figure 23** displays well-defined antenna pattern printed on photo paper with

prepared Cu NPs paste. The dipole tag antenna performance of printed patterns was investigated using the radio-frequency (RF) network analyzer with SMA-type connector. The performance of dipole tag antenna could be confirmed by bandwidth, voltage standing wave ratio (VSWR) and return loss (RL).[76, 77] Cu NPs paste-based dipole tag antenna displayed sharp peak of RL at 1.90 GHz and bandwidth of 0.16 GHz, from 1.82 to 1.98 GHz for 30 dB standard, as presented in **Figure 23.** These features indicate the Cu NPs paste is fully applicable to dipole tag antennas.

3.3. Fabrication of Sinter-free Conductive Paste using Cu NP and Cu NW composite

3.3.1. Fabrication of copolymer treated copper nanoparticles (CP-Cu NPs) and Cu nanowires (Cu NWs)

Figure 24 displays the TEM and SEM images of fabricated Cu NPs and Cu NWs. **Figure 24a and b** display the TEM images of fabricated Cu NPs. The synthesized Cu NPs were 10 nm in diameter and in monodispersed state. Cu NPs were fabricated by the previously reported method using copper acetate, isopropanolamine and hydrazine monohydrate.[78] Fabricated Cu NPs were treated with copolymer, poly(VI-co-VTS), to grant the Cu NPs with anti-oxidation ability. The fabricated Cu NPs were dispersed in mixture of ethanol and water. For complete dispersion, the Cu NPs were first sonicated in batch-sonicator for 5 min, and magnetically stirred for 15 min. Then, small amount of hydrochloric acid and phosphoric acid were added in the solution while stirred and left for 20 min. Hydrochloric acid were added to wash away the copper oxide residue and phosphoric acid passivates the copper surface to prevent further oxidation. After the acid treatment, the

copolymer solution was added in the above solution and stirred for 30 min to treat the copper surface with copolymer. Then, the solution was washed with acetone many times to wash away the acid and unreacted residues to obtain copolymer treated copper nanoparticles (CP-Cu NPs). The silane groups and imidazole ring binds to the Cu surface to prevent the oxidation of Cu NPs for high conductivity.

Figure 24c and d illustrates the TEM and SEM image of fabricated Cu NWs. It is confirmed that Cu NWs were synthesized with diameter of 80 nm average. Copper nanowires (Cu NWs) were fabricated by modifying the previously reported method. Copper chloride, hexadecylamine (HDA), and glucose were used in the synthesis process as copper precursor, surfactant, and reducing agent respectively.[79] Copper chloride, HDA, and glucose were dissolved in distilled water for 8 hrs. Then the solution was placed in steel autoclave and reacted for 24 hrs at 120 °C. Then the resultant solution was washed sequentially with water, hexane, and ethanol to remove the unreacted residue. Cu NWs were stored in glass bial and capped to prevent the surface oxidation.

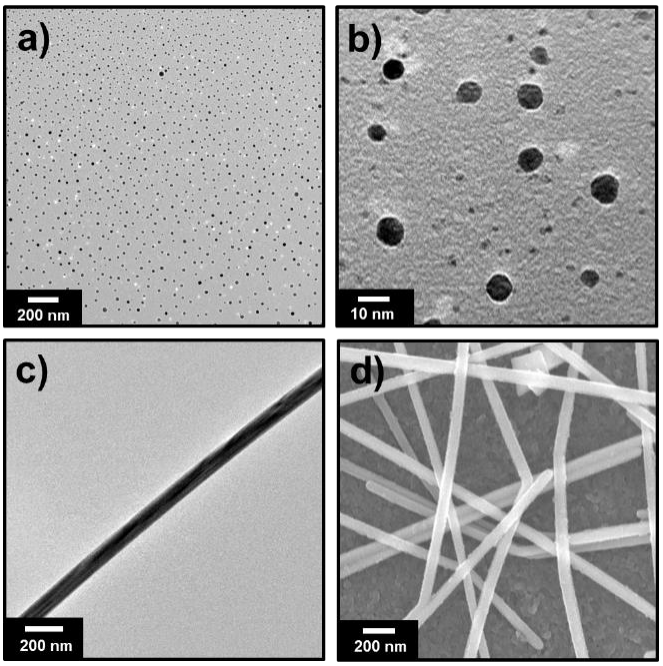

Figure 24. TEM images of **a),b)** Cu NPs, **c)** Cu NW and **d)** SEM image of Cu NWs.

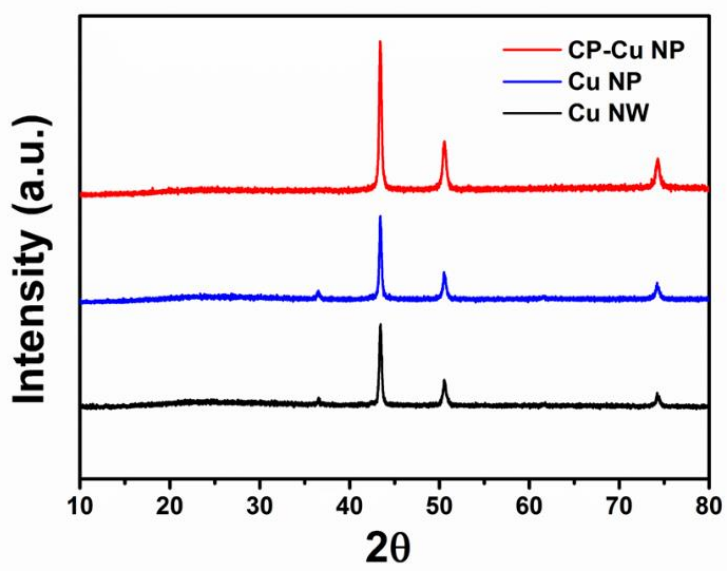

Figure 25. a) Fabrication procedure and **b)** FT-IR image of Poly(VI-co-VTS)

3.3.2. Characterization of Cu NP/NW Paste

To scrutinize the fabricated Cu NP, Cu NW, and CP-Cu NPs, X-ray diffraction (XRD) spectra were obtained for each materials **(Figure 25)**. XRD spectra for Cu NP, Cu NW, and CP-Cu NPs all exhibited sharp diffraction peaks at 2θ angles of 43.5, 50.7, and 74.3 °, which refers to the crystal planes of face-centered cubic (fcc) of crystalline copper.[6] The small peak which appears around 2θ angles of 36 ° refers to the small amount of Cu_2O arise from the surface of the copper.

Previous research used only CP-Cu NPs as solid-loadings to make sinter free conductive paste. However, numerous particle interface makes it hard for charge to travel through the paste. Therefore, Cu NWs, 1-D structured copper nanomaterials, were introduced to enhance the charge transport ability of sinter free conductive paste. In the case of Cu NPs paste, electron have hard time moving through numerous particle interface, non-conducting polymer, and ethyl cellulose (EC). However, Cu NW could provide electron with the efficient and fast travel route across the conductive paste, enhancing the conductivity of the paste. The Cu NP paste could form conductive network between NPs without sintering process due to the extremely small size of Cu NPs leading to

minimized size of the void. In case of Cu NWs paste, as Cu NW possess large diameter (≈80 nm), the large void arise within the Cu NW paste, which is why it exhibits higher resistivity than Cu NP paste without sintering.[80, 81] However, even though Cu NWs could not create highly conductive network without sintering process, it could increase the conductivity of the Cu NPs paste by mixed in with small amount. **Figure 26** illustrates how Cu NWs could increase the conductivity of the sinter free Cu NPs paste. The Cu NW mixed with the Cu NPs could work as the bridge for charge-transfer within the conductive paste, which could lead to increased conductivity.[22, 82, 83] However, if too much Cu NW is added to the Cu NPs paste, the conductivity might drop due to the increased number of large void.

Therefore, the weight ratio of the Cu NWs in the Cu conductive paste was adjusted to find appropriate ratio to minimize the resistivity of the conductive film. **Table 4** exhibits the composition of the fabricated Cu conductive paste. Cu conductive paste was made by mixing ethyl cellulose (EC), ethylene glycol butyl ether (EGBE), and CP-Cu NPs or Cu NWs for certain ratio. EC and EGBE act as matrix polymer and solvent respectively. The content of Cu NWs within solid loadings was

controlled by 10, 20, and 30 wt%, and solid loadings and base paste were mixed with weight ratio of 2:1. **Table 5** presents the thickness and resistivity of the conductive film printed using various Cu conductive paste. The conductive paste only made of Cu NW displayed much higher resistivity than the paste made of only Cu NPs. Cu NW paste-film showed resistivity of $3.58 \cdot 10^{-2}$ Ω·cm, which is almost 3 times higher than that of Cu NPs paste-film ($1.21 \cdot 10^{-2}$ Ω·cm). The content of the Cu NW in Cu NP/NW paste was adjusted to certain ratio. Among the fabricated Cu NP/NW paste, paste with Cu NW content of 10 and 20 wt% (Cu NP/NW 10, Cu NP/NW 20) displayed the higher conductivity than CP-Cu NP paste, indicating that Cu NW could improve the conductivity of the copper conducive paste. However, conductive paste with the Cu NW content of 30 wt% (Cu NP/NW 30) exhibited the highest resistivity among Cu NP/NW paste due to the increased number of large void within the conductive paste.

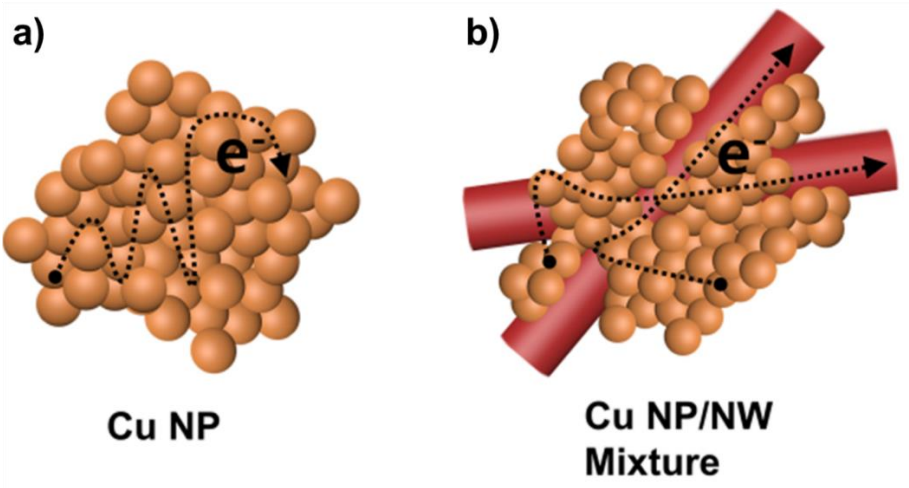

Figure 26. Schematic image of charge transport within Cu NPs paste and Cu NP/NW paste

Table 4. Composition of various synthesized Cu conductive paste

	Solid Loadings (wt%)		Base Paste (wt%)	
	CP-Cu NP	**Cu NW**	**EC**	**EGBE**
CP-Cu NP	100	0	25	75
Cu NW	0	100		
Cu NP/NW 10	90	10		
Cu NP/NW 20	80	20		
Cu NP/NW 30	70	30		

Table 5. Thickness and resistivity of the various synthesized Cu conductive paste

	Thickness	**Resistivity (Ω·cm)**
CP-Cu NP	120	$1.21 \cdot 10^{-2}$
Cu NW	140	$3.58 \cdot 10^{-2}$
Cu NP/NW 10	112	$1.02 \cdot 10^{-2}$
Cu NP/NW 20	104	$0.57 \cdot 10^{-2}$
Cu NP/NW 30	103	$1.54 \cdot 10^{-2}$

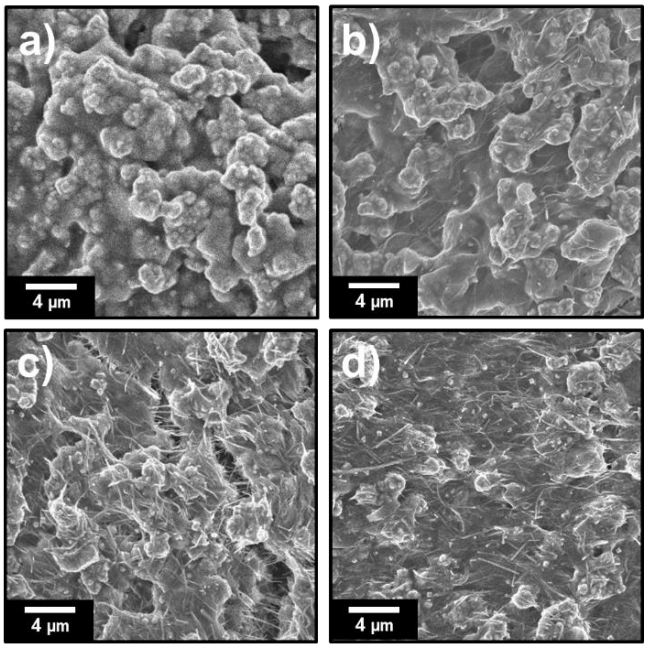

Fig 27. SEM images of Cu based conductive paste; **a)** Cu NP paste, **b)** Cu NP/NW 10, **c)** Cu NP/NW 20, and **d)** Cu NP/NW 30

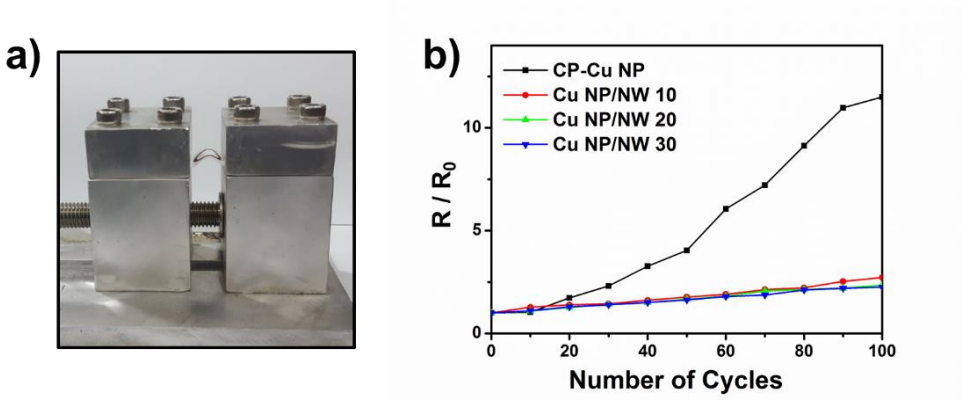

Figure 28. a) Photo of bended printed pattern and **b)** bending fatigue test of various synthesized Cu-based conductive paste

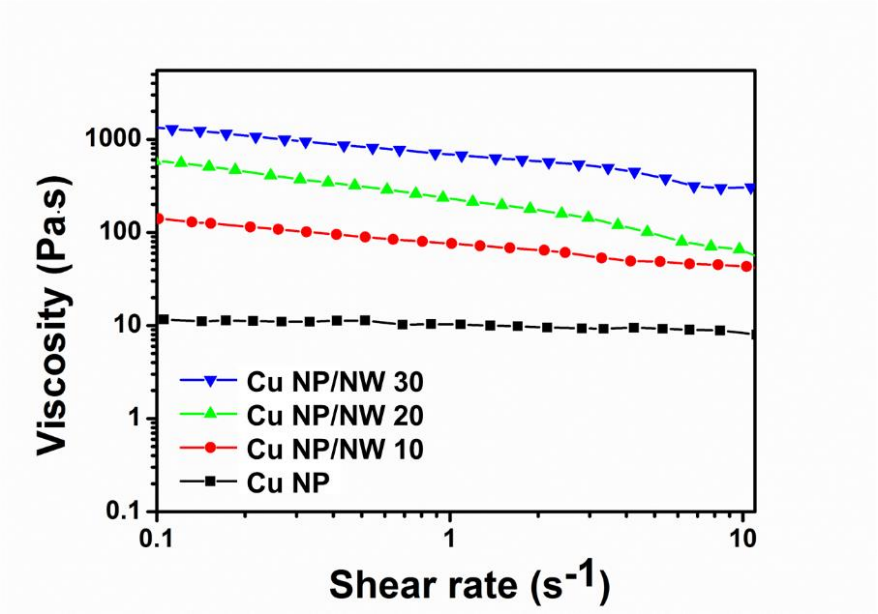

Figure 29. viscosity of printed pattern of various synthesized Cu-based conductive paste as a function of shear rate

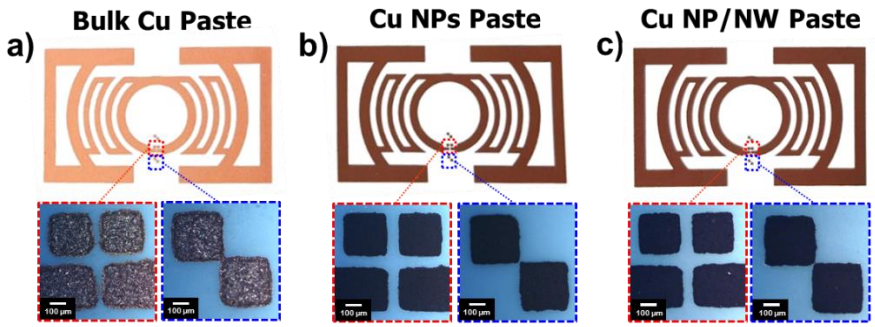

Figure 30. Pattern for dipole tag-antenna with optical image for enlarged section using **a)** bulk-copper paste and **b)** Cu NP paste and **c)** Cu NP/NW paste

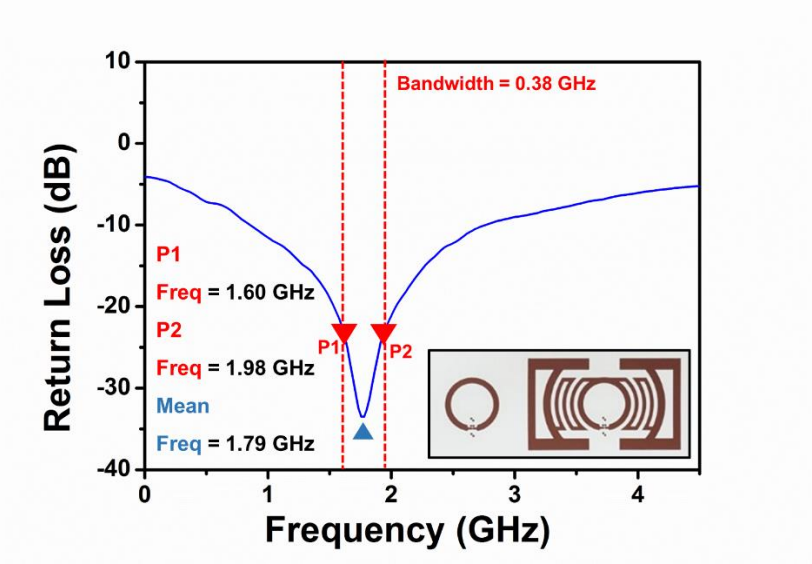

Figure 31. Return loss curve of the dipole tag antenna using Cu NP/NW 20 Paste-based electrode (inset: Printed antenna pattern using Cu NP/NW 20 Paste)

The increase of conductivity was analyzed through addition of Cu NWs in the conductive paste through SEM image. **Figure 27** exhibits the SEM images of the fabricated copper conductive paste. **Figure 27a** displays the surface of the CP-Cu NPs paste film and **Figure 27b, c and d** refers to the film printed with Cu conductive paste with Cu NW content of 10, 20, and 30 wt% (Cu NP/NW 10, Cu NP/NW 20, Cu NP/NW 30) respectively. It is confirmed that Cu NWs perform the role of charge-bridge between the cluster of Cu NPs. These bridge could connect the Cu NPs to enhance the conductivity of the Cu conductive film.

The bending fatigue test were held to investigate the stability of Cu NP/NW film. Bending stability is essential property for flexible conductive film. **Figure 28a** illustrates how bending fatigue test are held. The film printed using various Cu conductive paste are bent for bending radius of 15 mm for 100 times. **Figure 28b** exhibits how the resistivity of the film changes with increased time of bending, where R_0 and R indicates the initial and measured resistivity respectively. The R/R_0 value of the CP-Cu NP paste film highly increased due to the crack made from the repeated bending, reaching 11.5 after bent for 100 times. However, Cu NP/NW paste presented lower R/R_0 value compared to the film only

used Cu NPs. Cu NP/NW paste film exhibited the R/R_0 value of 2.72, 2.35, and 2.25 for Cu NP/NW 10, Cu NP/NW 20, and Cu NP/NW 30 respectively after 100 bending. Mixing Cu NWs could prevent the crack initiation, and connect the copper particles together even if the film is cracked.[84] The stability increased with the increased amount of Cu NWs in the conductive film. However, addition of Cu NWs should be controlled as the resistivity of the Cu conductive film largely increase from certain point with more Cu NWs added. Therefore, it can be concluded that Cu NP/NW 20 exhibits best performance in that it displays highest conductivity with high bending stability.

Viscosity is another important factor for conductive paste for flexible film. The viscosity of the conductive paste should be controlled to certain range of value for each application.[70, 71] Therefore, viscosity data for each copper conductive paste was measured controlling the shear rate. **Figure 29** illustrates the plots of viscosity of copper conductive paste with different Cu NW content by shear rate. The overall viscosity increased with larger amount of Cu NW mixed within the conductive paste. Cu NWs connects the cluster of Cu NPs together in every direction, leading to increased viscosity of the Cu NP/NW paste. Therefore, the

amount of Cu NWs added could be one of the factor to control the viscosity of the Cu NP/NW paste. **Figure 30** displays optical image of dipole tag-antenna pattern printed with bulk copper paste, Cu NPs paste, and Cu NP/NW paste. Cu NP/NW illustrates high-resolution line pattern as well as Cu NP paste.

In order to confirm the performance of Cu NP/NW paste for actual application, it is employed in the dipole tag antenna pattern. The antenna pattern was prepared on a flexible substrate using the screen printing method with film thickness of 40 μm. The inset image in **Figure 31** displays well-defined pattern printed on photo paper with prepared Cu NP/NWs paste. The dipole tag antenna performance of printed patterns was investigated using the radio-frequency (RF) network analyzer with SMA-type connector. Cu NPs paste-based dipole tag antenna displayed sharp peak of RL at 1.79 GHz and bandwidth of 0.38 GHz, from 1.60 to 1.98 GHz for 23 dB standard. These features indicate the Cu NP/NWs paste is applicable to dipole tag antennas.

4. Conclusion

The sinter-free conductive paste based on Cu NPs and Cu NWs were successfully fabricated. Cu NW paste, Cu NP paste, and Cu NP/NW paste exhibited enhanced conductivity, thermal stability, and bending stability. Fabricated conductive paste were applied to glucose sensor, and dipole tag antenna to and exhibited its applicability to various applications. The subtopics could be summarized as follows:

1. Cu NWs paste were fabricated to substitute intrinsically low-conductive carbon paste. Cu NWs were synthesized through hydrothermal method and used as solid loadings for the Cu NW paste. Synthesized Cu NWs and Cu NW paste exhibited the existence of fcc structure of Cu. Also, Cu NW paste displayed lower resistivity of $3.58 \cdot 10^{-2}$ Ω·cm compared to conventional carbon paste ($9.71 \cdot 10^{-2}$ Ω·cm) even without thermal sintering.
2. To improve the conductivity and thermal stability of the copper nanostructure based sinter-free conductive paste, CP-Cu NPs were employed in the conductive paste. Sub-10 nm Cu NPs were synthesized

as solid loadings for the conductive paste, and coated with poly(VI-co-VTS) to fabricate CP-Cu NPs. CP-Cu NPs exhibited high thermal stability up to 300 °C. Cu NPs paste were composed of CP-Cu NPs, EC, and EGBE. Cu NP paste displayed lower resistivity of $1.21 \cdot 10^{-2}$ Ω·cm compared to Cu NW paste due to the small size of void between the solid loadings even without thermal sintering process. The Cu NPs paste were employed as dipole tag antenna pattern and showed applicability as conductive paste.

3. To improve the conductivity and bending stability of the Cu NPs paste, Cu NWs were employed in the conductive paste to fabricate Cu NP/NW paste. Added Cu NW could provide electron with efficient and fast travel route across the conductive paste. Cu NP/NW 20 exhibited low resistivity of $0.57 \cdot 10^{-2}$ Ω·cm. Also, Cu NWs could prevent the crack initiation and connect the Cu NPs together even if the film is bent, leading to high bending stability. Cu NP/NW paste showed lower R/R_0 value of 2.35 compared to the film only used Cu NPs (11.5) while the film is bent for 100 times in bending fatigue test. The Cu NP/NW paste were employed as dipole tag antenna pattern and displayed applicability as conductive paste.

References

[1] S. D. Senanayake, D. Stacchiola and J. A. Rodriguez, *Acc. Chem. Res.*, **2013**, 46, 1702.

[2] D. H. Atha, H. Wang, E. J. Petersen, D. Cleveland, R. D. Holbrook, P. Jaruga, M. Dizdaroglu, B. Xing and B. C. Nelson, *Environ. Sci. Technol.*, **2012**, 46, 1819.

[3] B. Bagchi, S. Kar, S. K. Dey, S. Bhandary, D. Roy, T. K. Mukhopadhyay, S. Das and P. Nandy, *Colloids and Surfaces B: Biointerfaces*, **2013**, 108, 358.

[4] M. R. Decan, S. Impellizzeri, M. Luisa Marin and J. C. Scaiano, *Nature Communications*, **2014**, 5.

[5] B. Kang, S. Han, J. Kim, S. Ko and M. Yang, *Journal of Physical Chemistry C*, **2011**, 115, 23664.

[6] D. Deng, Y. Jin, Y. Cheng, T. Qi and F. Xiao, *ACS Applied Materials and Interfaces*, **2013**, 5, 3839.

[7] Y. Lee, J. R. Choi, K. J. Lee, N. E. Stott and D. Kim, *Nanotechnology*, **2008**, 19.

[8] B. K. Park, D. Kim, S. Jeong, J. Moon and J. S. Kim, *Thin Solid Films*, **2007**, 515, 7706.

[9] T. M. D. Dang, T. T. T. Le, E. Fribourg-Blanc and M. C. Dang, *Advances in Natural Sciences: Nanoscience and Nanotechnology*, **2011**, 2.

[10] M. Jin, G. He, H. Zhang, J. Zeng, Z. Xie and Y. Xia, *Angewandte Chemie - International Edition*, **2011**, 50, 10560.

[11] H. Ohde, F. Hunt and C. M. Wai, *Chem. Mater.*, **2001**, 13, 4130.

[12] B. K. Park, S. Jeong, D. Kim, J. Moon, S. Lim and J. S. Kim, *J. Colloid Interface Sci.*, **2007**, 311, 417.

[13] L. Qi, J. Ma and J. Shen, *J. Colloid Interface Sci.*, **1997**, 186, 498.

[14] M. B. Gawande, A. Goswami, F.-X. Felpin, T. Asefa, X. Huang, R. Silva, X. Zou, R. Zboril and R. S. Varma, *Chem. Rev.*, **2016**, 116, 3722.

[15] S. Qiu, J. Dong and G. Chen, *J. Colloid Interface Sci.*, **1999**, 216, 230.

[16] H. Kawasaki, Y. Kosaka, Y. Myoujin, T. Narushima, T. Yonezawa and R. Arakawa, *Chem. Commun.*, **2011**, 47, 7740.

[17] H.-t. Zhu, C.-y. Zhang and Y.-s. Yin, *J. Cryst. Growth*, **2004**, 270, 722.

[18] Z. Liu and Y. Bando, *Adv. Mater.*, **2003**, 15, 303.

[19] A. R. Rathmell, S. M. Bergin, Y. L. Hua, Z. Y. Li and B. J. Wiley, *Adv. Mater.*, **2010**, 22, 3558.

[20] H. Wu, L. Hu, M. W. Rowell, D. Kong, J. J. Cha, J. R. McDonough, J. Zhu, Y. Yang, M. D. McGehee and Y. Cui, *Nano Lett.*, **2010**, 10, 4242.

[21] D. Zhang, R. Wang, M. Wen, D. Weng, X. Cui, J. Sun, H. Li and Y. Lu, *J. Am. Chem. Soc.*, **2012**, 134, 14283.

[22] S. Bhanushali, P. Ghosh, A. Ganesh and W. Cheng, *Small*, **2015**, 11, 1232.

[23] Y. Chang, M. L. Lye and H. C. Zeng, *Langmuir*, **2005**, 21, 3746.

[24] M. Jin, G. He, H. Zhang, J. Zeng, Z. Xie and Y. Xia, *Angew. Chem. Int. Ed.*, **2011**, 50, 10560.

[25] Z. Liu, Y. Yang, J. Liang, Z. Hu, S. Li, S. Peng and Y. Qian, *The Journal of Physical Chemistry B*, **2003**, 107, 12658.

[26] Y.-Q. Liu, M. Zhang, F.-X. Wang and G.-B. Pan, *RSC Advances*, **2012**, 2, 11235.

[27] Y.-S. Cho and Y.-D. Huh, *Mater. Lett.*, **2009**, 63, 227.

[28] A. Teichler, J. Perelaer and U. S. Schubert, *Journal of Materials Chemistry C*, **2013**, 1, 1910.

[29] M. Singh, H. M. Haverinen, P. Dhagat and G. E. Jabbour, *Adv. Mater.*, **2010**, 22, 673.

[30] C. Gerard and P. Y. D. Marc, *Circuit World*, **2012**, 38, 193.

[31] S. Park, M. Vosguerichian and Z. Bao, *Nanoscale*, **2013**, 5, 1727.

[32] A. Kamyshny and S. Magdassi, *Small*, **2014**, 10, 3515.

[33] A. Kamyshny and S. Magdassi, in *Inkjet-Based Micromanufacturing*, Wiley-VCH Verlag GmbH & Co. KGaA, 2012, DOI: 10.1002/9783527647101.ch12, pp. 173.

[34] A. Kamyshny and S. Magdassi, in *Nanoscience*, CRC Press, 2010, DOI: doi:10.1201/EBK1420065008-c25

10.1201/EBK1420065008-c25, pp. 747.

[35] J. Perelaer, in *Inkjet-Based Micromanufacturing*, Wiley-VCH Verlag GmbH & Co. KGaA, 2012, DOI: 10.1002/9783527647101.ch8, pp. 111.

[36] F. M. Wolf, J. Perelaer, S. Stumpf, D. Bollen, F. Kriebel and U. S. Schubert, *J. Mater. Res.*, **2013**, 28, 1254.

[37] F. Wang, P. Mao and H. He, **2016**, 6, 21398.

[38] J. S. Lee, M. Kim, J. Oh, J. Kim, S. Cho, J. Jun and J. Jang, *Journal of Materials Chemistry A*, **2015**, 3, 7029.

[39] R. Prehn, M. Cortina-Puig and F. X. Muñoz, *J. Electrochem. Soc.*, **2012**, 159, F134.

[40] F. Meng, W. Shi, Y. Sun, X. Zhu, G. Wu, C. Ruan, X. Liu and D. Ge, *Biosens. Bioelectron.*, **2013**, 42, 141.

[41] B. D. Malhotra, A. Chaubey and S. P. Singh, *Anal. Chim. Acta*, **2006**, 578, 59.

[42] J. Wang, *Chem. Rev.*, **2008**, 108, 814.

[43] S. Park, S. Y. Lee, H. Boo, H.-M. Kim, K.-B. Kim, H. C. Kim, Y. J. Song and T. D. Chung, *Chem. Mater.*, **2007**, 19, 3373.

[44] Y. Sun, H. Buck and T. E. Mallouk, *Anal. Chem.*, **2001**, 73, 1599.

[45] S. Ammara, S. Shamaila, R. Sharif, S. Ghani and N. Zafar, *Acta Metallurgica Sinica (English Letters)*, **2016**, 29, 889.

[46] S. Jie, S. Honghui, C. Gang, Z. Yuting, Z. Yingying, X. Tiantian, J.

Hongmei and H. Yunbin, *Current Nanoscience*, **2015**, 11, 736.

[47] J. Dong, L. Ren, Y. Zhang, X. Cui, P. Hu and J. Xu, *Talanta*, **2015**, 132, 719.

[48] T. Yang, J. Xu, L. Lu, X. Zhu, Y. Gao, H. Xing, Y. Yu, W. Ding and Z. Liu, *J. Electroanal. Chem.*, **2016**, 761, 118.

[49] L. Ju, G. Wu, B. Lu, X. Li, H. Wu and A. Liu, *Electroanalysis*, **2016**, 28, 2543.

[50] N. Hui, W. Wang, G. Xu and X. Luo, *Journal of Materials Chemistry B*, **2015**, 3, 556.

[51] Q. Wang, Q. Wang, M. Li, S. Szunerits and R. Boukherroub, *RSC Advances*, **2015**, 5, 15861.

[52] Y. Zhang, L. Su, D. Manuzzi, H. V. E. de los Monteros, W. Jia, D. Huo, C. Hou and Y. Lei, *Biosens. Bioelectron.*, **2012**, 31, 426.

[53] X. Niu, Y. Li, J. Tang, Y. Hu, H. Zhao and M. Lan, *Biosens. Bioelectron.*, **2014**, 51, 22.

[54] J. Zhao, L. Wei, C. Peng, Y. Su, Z. Yang, L. Zhang, H. Wei and Y. Zhang, *Biosens. Bioelectron.*, **2013**, 47, 86.

[55] J. Huang, Z. Dong, Y. Li, J. Li, J. Wang, H. Yang, S. Li, S. Guo, J. Jin and R. Li, *Sensors and Actuators B: Chemical*, **2013**, 182, 618.

[56] D. Jiang, Q. Liu, K. Wang, J. Qian, X. Dong, Z. Yang, X. Du and B. Qiu, *Biosens. Bioelectron.*, **2014**, 54, 273.

[57] Y. Zhao, Z. He and Z. Yan, *Analyst*, **2013**, 138, 559.

[58] Y. Hokita, M. Kanzaki, T. Sugiyama, R. Arakawa and H. Kawasaki, *ACS Appl. Mater. Interfaces*, **2015**, 7, 19382.

[59] T. Yonezawa, H. Tsukamoto, Y. Yong, M. T. Nguyen and M. Matsubara, *RSC Advances*, **2016**, 6, 12048.

[60] Y. Yong, T. Yonezawa, M. Matsubara and H. Tsukamoto, *Journal of Materials Chemistry C*, **2015**, 3, 5890.

[61] K. Cheirmadurai, S. Biswas, R. Murali and P. Thanikaivelan, *RSC*

Advances, **2014**, 4, 19507.

[62] H. J. Kim, Y. J. Park, J.-H. Choi, H. S. Han and Y. T. Hong, *Journal of Industrial and Engineering Chemistry*, **2009**, 15, 23.

[63] G. Pappalardo, G. Impellizzeri, R. P. Bonomo, T. Campagna, G. Grasso and M. G. Saita, *New Journal of Chemistry*, **2002**, 26, 593.

[64] M. Zhang, C. Guan and W. Wang, *Corrosion Science and Protection Technology*, **2001**, 13, 96.

[65] H. Kim and J. Jang, *Polymer*, **1998**, 39, 4065.

[66] T. Dahlang and T. Sven, *J. Phys.: Condens. Matter*, **2012**, 24, 175002.

[67] F. A. Akgul, G. Akgul, N. Yildirim, H. E. Unalan and R. Turan, *Mater. Chem. Phys.*, **2014**, 147, 987.

[68] B. Wang, H.-J. Liu and Y. Chen, *RSC Advances*, **2016**, 6, 2141.

[69] Y. Dong, H. Pang, H. B. Yang, C. Guo, J. Shao, Y. Chi, C. M. Li and T. Yu, *Angewandte Chemie International Edition*, **2013**, 52, 7800.

[70] D. Tobjörk and R. Österbacka, *Adv. Mater. (Weinheim, Ger.)*, **2011**, 23, 1935.

[71] P. G. Karagiannidis, S. A. Hodge, L. Lombardi, F. Tomarchio, N. Decorde, S. Milana, I. Goykhman, Y. Su, S. V. Mesite, D. N. Johnstone, R. K. Leary, P. A. Midgley, N. M. Pugno, F. Torrisi and A. C. Ferrari, *ACS Nano*, **2017**, 11, 2742.

[72] A. Benchabane and K. Bekkour, *Colloid Polym. Sci.*, **2008**, 286, 1173.

[73] S. Hemmati, D. P. Barkey and N. Gupta, *Journal of Nanoparticle Research*, **2016**, 18, 249.

[74] Q. Xue, *Eur. Polym. J.*, **2004**, 40, 323.

[75] H. Guo, N. Lin, Y. Chen, Z. Wang, Q. Xie, T. Zheng, N. Gao, S. Li, J. Kang, D. Cai and D. L. Peng, *Scientific Reports*, **2013**, 3.

[76] M. Kubo, X. Li, C. Kim, M. Hashimoto, B. J. Wiley, D. Ham and G. M. Whitesides, *Adv. Mater. (Weinheim, Ger.)*, **2010**, 22, 2749.

[77] K. Y. Shin, S. Cho and J. Jang, *Small*, **2013**, 9, 3792.

[78] Y. Hokita, M. Kanzaki, T. Sugiyama, R. Arakawa and H. Kawasaki, *ACS Applied Materials & Interfaces*, **2015**, 7, 19382.

[79] M. Mohl, P. Pusztai, A. Kukovecz, Z. Konya, J. Kukkola, K. Kordas, R. Vajtai and P. M. Ajayan, *Langmuir*, **2010**, 26, 16496.

[80] Y. Kim, B. Lee, S. Yang, I. Byun, I. Jeong and S. M. Cho, *Current Applied Physics*, **2012**, 12, 473.

[81] R. Wang and H. Ruan, *J. Alloys Compd.*, **2016**, 656, 936.

[82] A. R. Rathmell, S. M. Bergin, Y.-L. Hua, Z.-Y. Li and B. J. Wiley, *Adv. Mater.*, **2010**, 22, 3558.

[83] T.-H. Duong, N.-H. Tran and H.-C. Kim, *Thin Solid Films*, **2017**, 622, 17.

[84] S.-J. Joo, S.-H. Park, C.-J. Moon and H.-S. Kim, *ACS Applied Materials & Interfaces*, **2015**, 7, 5674.

국문초록

인쇄전자기술은 전자 기기의 제조에서 유망한 기술 중 하나로 꼽히고 있다. 특히, 다양한 응용이 가능하다는 점에서 유연성 전자제품에서 각광받고 있는 기술이다. 기존의 제조기술은 값비싼 장비와 높은 비용의 제조기술을 요구한다. 이로 인하여 전도성 페이스트/잉크를 사용하는 인쇄전자기술이 값싸고 빠르다는 점에서 주목받고 있다. 전도성 페이스트는 주로 전도성 물질과 액체 베이스, 그리고 다양한 첨가제로 이루어진다. 특히 금속 나노물질은 최근 대량 생산을 가능케 한 습식 화학 합성법으로 인하여 많은 관심을 받고있다. 특히 은 나노입자 기반 전도성 페이스트는 높은 전도성으로 인하여 널리 사용되어 왔다. 하지만 은의 높은 가격으로 인하여 은 기반 전도성 페이스트의 실생활 응용이 힘들었다.

본 학위논문에서는 저렴한 구리나노물질을 이용한 전도성 페이스트의 제조법을 제시하였다. 또한 본 논문에서 제시한 전도성 페이스트는 추가적인 열이나 빛을 이용한 소결 공정을 필요로 하지 않아 제조비용을 절감할 수 있으며,

열이나 빛에 약한 서브스트레이트의 활용 또한 가능하다. 구리 나노입자와 나노섬유는 습식 화학적 합성법과 수열 합성법을 통하여 제조되었다. 구리 나노섬유는 기존의 탄소 기반 페이스트를 대체하는 이중 기능 물질(글루코오스 센서와 전도성페이스트)로 활용되었다. 구리 나노입자는 비소결식 전도성 페이스트의 전도성을 향상시키기 위해서 활용되었으며, 구리나노입자와 나노섬유를 조합함으로써 전도성을 향상시키는 연구 또한 포함된다.

본 논문에서 제시한 비소결식 전도성 페이스트는 회로 기판, RFID 태그, 박막 트랜지스터, 발광 다이오드, 태양전지, 투명 전극, 플렉시블 디스플레이 등에 활용될 수 있다. 또한 본 학위논문은 구리 나노물질 기반 전도성 페이스트의 제조법을 제시할 뿐만 아니라, 새로운 비소결식 전도성 페이스트의 제조에 관한 아이디어를 제시한다.

주요어: 구리 나노입자, 전도성 페이스트, 비소결식 공정, 플렉시블 전극, 글루코오스 센서, 다이폴 태그 안테나
학 번: 2013-22534